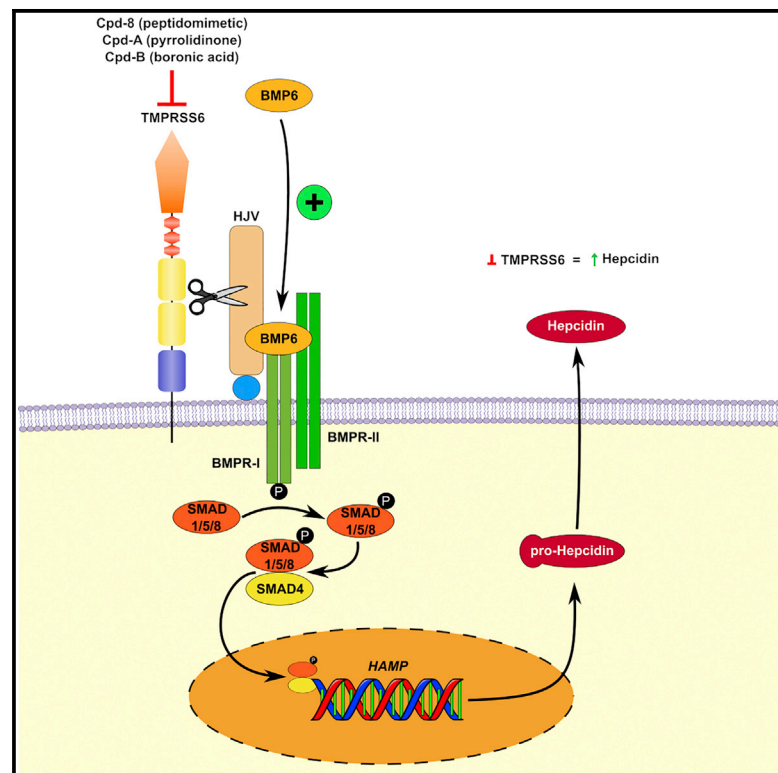


# Cell Chemical Biology

## Discovery and Development of TMPRSS6 Inhibitors Modulating Hepcidin Levels in Human Hepatocytes

### Graphical Abstract



### Authors

François Béliveau, Aarti Tarkar,  
 Sébastien P. Dion, ...,  
 Michael Ouellette, Andrew J. Pope,  
 Richard Leduc

### Correspondence

richard.leduc@usherbrooke.ca

### In Brief

TMPRSS6 is a human liver enzyme considered as a therapeutic target for iron overload-related diseases, such as hereditary hemochromatosis and  $\beta$ -thalassemia. In this study, Béliveau et al. discovered and characterized three different classes of TMPRSS6 inhibitors that increase production of hepcidin, the major iron regulatory hormone, in human hepatocytes.

### Highlights

- Discovery of TMPRSS6 inhibitors from high-throughput screening
- *In cellulo* characterization of peptidomimetic and non-peptidic inhibitors of TMPRSS6
- Inhibitors abolish TMPRSS6-mediated HJV cleavage
- Inhibitors upregulate hepcidin production in human hepatocytes

# Discovery and Development of TMPRSS6 Inhibitors Modulating Hepcidin Levels in Human Hepatocytes

François Béliveau,<sup>1,2</sup> Aarti Tarkar,<sup>3</sup> Sébastien P. Dion,<sup>1,2</sup> Antoine Désilets,<sup>1,2</sup> Mariana Gabriela Ghinet,<sup>1,2</sup> Pierre-Luc Boudreault,<sup>1,2</sup> Catherine St-Georges,<sup>1,2</sup> Éric Marsault,<sup>1,2</sup> Daniel Paone,<sup>3</sup> Jon Collins,<sup>3</sup> Colin H. Macphee,<sup>3</sup> Nino Campobasso,<sup>4</sup> Arthur Groy,<sup>4</sup> Josh Cottom,<sup>4</sup> Michael Ouellette,<sup>4</sup> Andrew J. Pope,<sup>3</sup> and Richard Leduc<sup>1,2,5,\*</sup>

<sup>1</sup>Department of Pharmacology-Physiology, Faculty of Medicine and Health Sciences, Université de Sherbrooke, 3001, 12<sup>e</sup> Avenue Nord, Sherbrooke, QC J1H 5N4, Canada

<sup>2</sup>Institut de Pharmacologie de Sherbrooke, Université de Sherbrooke, Sherbrooke, QC, Canada

<sup>3</sup>Discovery Partnerships with Academia, GlaxoSmithKline, Collegeville, Philadelphia, PA 19426-0989, USA

<sup>4</sup>Platform Technology & Science, GlaxoSmithKline, Collegeville, Philadelphia, PA 19426-0989, USA

<sup>5</sup>Lead Contact

\*Correspondence: [richard.leduc@usherbrooke.ca](mailto:richard.leduc@usherbrooke.ca)

<https://doi.org/10.1016/j.chembiol.2019.09.004>

## SUMMARY

Iron overload disorders are characterized by the body's inability to regulate iron absorption and its storage which can lead to organ failures. Accumulated evidence has revealed that hepcidin, the master regulator of iron homeostasis, is negatively modulated by TMPRSS6 (matriptase-2), a liver-specific type II transmembrane serine protease (TTSP). Here, we report that treatment with a peptidomimetic inhibitor affecting TMPRSS6 activity increases hepcidin production in hepatic cells. Moreover, similar effects were observed when using non-peptidic inhibitors obtained through optimization of hits from high-throughput screening. Using HepG2 cells and human primary hepatocytes, we show that TMPRSS6 inhibitors block TMPRSS6-dependent hemojuvelin cleavage and increase *HAMP* expression and levels of secreted hepcidin.

## INTRODUCTION

Type II transmembrane serine proteases (TTSPs) are proteolytic enzymes localized at the plasma membrane that share conserved domains. They possess an amino-terminal cytoplasmic region, a single-pass transmembrane domain, and an extracellular domain composed of various regions ultimately ending with a C-terminal serine protease catalytic domain (Antalis et al., 2011; Hooper et al., 2001). According to the MEROPS peptidase database (Rawlings et al., 2018), TTSPs belong to the chymotrypsin-fold PA clan of proteases and are part of the S1 subfamily. TMPRSS6, also known as matriptase-2, is a TTSP almost exclusively expressed at the surface of hepatocytes in the liver (Dion et al., 2018a; Ramsay et al., 2008) and plays a key role in iron homeostasis via modulation of hepcidin expression (Du et al., 2008; Finberg et al., 2008; Folgueras et al., 2008; Silvestri et al., 2008a).

The role of TMPRSS6 in iron regulation was first revealed by association of *TMPRSS6* genetic mutations found in patients suffering from iron-refractory iron deficiency anemia (IRIDA), a condition associated with low circulating iron, elevated hepcidin levels and unresponsiveness to oral iron therapy (Finberg et al., 2008). Concomitantly, a chemically induced mutant mouse model (*mask*) exhibiting microcytic anemia where a splicing defect led to the production of a catalytically inactive TMPRSS6 protein was described (Du et al., 2008). A *Tmprss6*<sup>-/-</sup> mice model also confirmed that absence of the protease causes anemia associated with elevated hepcidin levels (Folgueras et al., 2008). In these models, loss of enzymatic function was associated with an increase in the serum levels of hepcidin, a secreted hepatic hormone that decreases the body's iron content through ferroportin (FPN) occlusion and degradation, resulting in IRIDA (Aschemeyer et al., 2018; Finberg et al., 2008).

At the cell surface, TMPRSS6 is a negative regulator of hepcidin production by acting at the apex of a bone morphogenetic protein/SMAD signaling pathway modulating expression of *HAMP*, the gene coding for hepcidin (Du et al., 2008; Nemeth et al., 2004). TMPRSS6 exerts its effect via cleavage of hemojuvelin (HJV), a co-receptor for the BMP family, which is an essential element, along with BMP receptors, transferrin receptor-2, and homeostatic iron regulator protein (Finberg et al., 2010; Silvestri et al., 2008a; Wahedi et al., 2017) contributing to iron homeostasis. Therefore, it can be postulated that inhibition of TMPRSS6 may result in increased hepcidin levels, making it a potentially attractive pharmacological target for diseases characterized by iron overload such as thalassemias and hemochromatosis (Beckmann et al., 2016a; Wang et al., 2014). Proof-of-concept for this idea has been demonstrated in pre-clinical model systems by knockout of the *TMPRSS6* gene or reduction of its mRNA expression using antisense oligonucleotides (ASOs). These approaches led to reduced iron levels and related symptoms (e.g., siderosis, quality of erythropoiesis) in mouse models of hemochromatosis and  $\beta$ -thalassemia (Casu et al., 2016; Finberg et al., 2011; Guo et al., 2013; Nai et al., 2012, 2014; Schmidt et al., 2013). Recently, small molecules (thiazolidinones) have been shown to reduce iron overload in mice models of hereditary hemochromatosis and  $\beta$ -thalassemia through hepcidin upregulation, by a mechanism involving

TMPRSS6 reduction at both the mRNA and protein levels (Liu et al., 2019). While these compounds are not direct protease inhibitors, it warrants the use of small molecules targeting TMPRSS6 in a therapeutic context.

Like other serine proteases, TTSPs have similar substrate specificities, each protease possessing distinct structural determinants (Barré et al., 2014; Béliveau et al., 2009). Because closely related TTSPs play essential physiological roles, for example matriptase regulates epithelial barrier formation and permeability in the intestine (Buzza et al., 2010), a highly selective TMPRSS6 inhibitor would be required to avoid potential side effects. Several groups including ours have reported on the development of different classes of TMPRSS6 inhibitors (Beckmann et al., 2016a, 2016b; Dosa et al., 2012; Duchêne et al., 2014; Gitlin et al., 2015; Häußler et al., 2016; Maurer et al., 2013; Roydeva et al., 2016; Sisay et al., 2010; St-Georges et al., 2017). However, many of these studies did not exhaustively address the compounds' selectivity for TMPRSS6 over other TTSPs or serine proteases in general. Highly potent (low nM  $K_i$ ) and selective (>60-fold selectivity for TMPRSS6 over matriptase) peptidomimetic inhibitors using unnatural amino acids and a ketobenzothiazole serine trap (St-Georges et al., 2017) currently exist but those compounds have only been characterized *in vitro*.

Here, we report that a previously developed peptidomimetic compound with low nanomolar  $K_i$  and >10-fold selectivity for TMPRSS6 over matriptase inhibits TMPRSS6 proteolytic activity in transfected cells and modulates the BMP6-hepcidin pathway in cellular models. In addition, we performed high-throughput screening campaigns to identify non-peptidomimetic compounds. This led to the identification and characterization of two distinct additional chemical classes of TMPRSS6 inhibitors, i.e., pyrrolidinones and boronic acids. Using the immortalized hepatocellular carcinoma cell line HepG2 as well as human primary hepatocytes, we demonstrate that exemplar compounds from all three classes significantly reduce TMPRSS6-dependent HJV cleavage as well as increase *HAMP* expression and hepcidin levels.

## RESULTS

### Benzothiazole-Based Peptidomimetics Compounds Inhibit TMPRSS6 *In Cellulo*

We previously developed a series of peptidomimetic inhibitors of TMPRSS6 with a generic scaffold composed of a ketobenzothiazole serine trap at the C terminus flanked by an arginine in P1, and in which positions P4, P3, and P2 were varied using unnatural amino acids (St-Georges et al., 2017) (Figure 1A). These compounds were characterized *in vitro* using recombinant human TMPRSS6 and matriptase to determine  $K_i$  values and selectivity, but their effects in cellular assays were never evaluated. To assess their ability at inhibiting TMPRSS6 activity *in cellulo*, we selected the most potent and specific TMPRSS6 compounds. Those with  $K_i < 5$  nM and a 10-fold selectivity over matriptase were chosen. A total of 12 compounds respecting those conditions were initially selected (Table S1).

To evaluate the inhibitory effects of these compounds on TMPRSS6 activity *in cellulo*, we transfected HEK293 cells with TMPRSS6 and its catalytically inactive counterpart (TMPRSS6

S762A; Figure 1B). Inhibitors (100 nM) or vehicle (DMSO) were added 24 h post transfection and cell media were collected after a 24-h incubation. Proteolytic activity was evaluated using a TMPRSS6 fluorogenic peptide substrate. Of the 12 compounds tested, three; compounds **2** ((H)Y-Y-V-R-kbt), **8** ((H)F-(thiazol-4-yl)alanine-V-R-kbt), and **29** ((H)F-hF-(Allo)T-R-kbt) (Cpd-**2**, **-8**, and **-29**) (chemical structures in Figure S1) showed significantly lower residual TMPRSS6 proteolytic activity compared with untreated cells and comparable activity with cells transfected with the catalytically inactive mutant (S762A). Noteworthy, Cpd-**1** (Y-Y-V-R-kbt), the only non-desamino compound tested, did not exhibit TMPRSS6 inhibition in transfected cells. This compound was shown to be unstable in mouse plasma (St-Georges et al., 2017), which may explain the absence of inhibition in treated cells.

We further evaluated the capacity of these three compounds (Cpd-**2**, **-8**, **-29**) to prevent TMPRSS6 shedding, an autocatalytic event (Stirnberg et al., 2010), in the same conditions (Figure 1C). Cpd-**1** and the catalytically inactive mutant S762A were used as controls. In the cell media of transfected and compound-treated cells, a significant decrease of the shed forms of TMPRSS6 (zymogen shed form, 110 kDa; active shed form, 32 kDa) was observed in cells treated with Cpd-**2** and **-8** and to a lesser extent with Cpd-**29**. Cpd-**1** did not have an effect and no cell surface shedding of TMPRSS6 was detected in cells transfected with the catalytically inactive mutant (Figure 1C).

To compare the potencies of the best compounds *in cellulo* toward TMPRSS6, we calculated half maximal inhibitory concentration ( $IC_{50}$ ) values for Cpd-**2**, **-8**, and **-29** in TMPRSS6-transfected HEK293 cells (Figure 1D). All three compounds displayed low nanomolar  $IC_{50}$ s, Cpd-**2** ( $4.75 \pm 1.47$  nM) and Cpd-**8** ( $7.65 \pm 1.86$  nM) being the most potent, followed by Cpd-**29** ( $43.1 \pm 17.7$  nM). No cytotoxicity was observable at the highest compound concentration used (10  $\mu$ M) (Figure S2A), and compounds did not negatively affect TMPRSS6 plasma membrane localization (Figure S3A), suggesting that reduction in activity was due to direct protease inhibition.

To gain information on compound selectivity, we calculated their  $IC_{50}$  values using various recombinant proteases *in vitro*. We first compared inhibitory activity toward TMPRSS6 and two closely related TTSPs (matriptase and hepsin). Matriptase is a potential off-target due to high similarity although it is not expressed in the liver according to the Human Protein Atlas (Uhlén et al., 2015), while hepsin is highly expressed in the liver (Table S2). We also tested the compounds against two serine proteases of the same protease clan and family (PA, S1) expressed in the liver (thrombin and factor Xa; Table S2), and furin, a serine protease known to be involved in HJV and hepcidin processing (Silvestri et al., 2008b; Valore and Ganz, 2008). As expected, all three compounds exhibit low nanomolar  $IC_{50}$  values for TMPRSS6 with values of 11 nM for Cpd-**2**, 8.1 nM for Cpd-**8**, and 25 nM for Cpd-**29** (Figure 1E for heatmap representation supported by Table S3). When compared with other TTSPs (matriptase and hepsin), Cpd-**2** and **-8** were not as potent, with  $IC_{50}$  values toward matriptase of 158 and 52 nM, and toward hepsin of 74 and 16 nM, respectively. Cpd-**29** is a weaker inhibitor of both matriptase ( $IC_{50} = 1.5$   $\mu$ M) and hepsin ( $IC_{50} = 0.4$   $\mu$ M). Interestingly, all three compounds were shown to be weak inhibitors

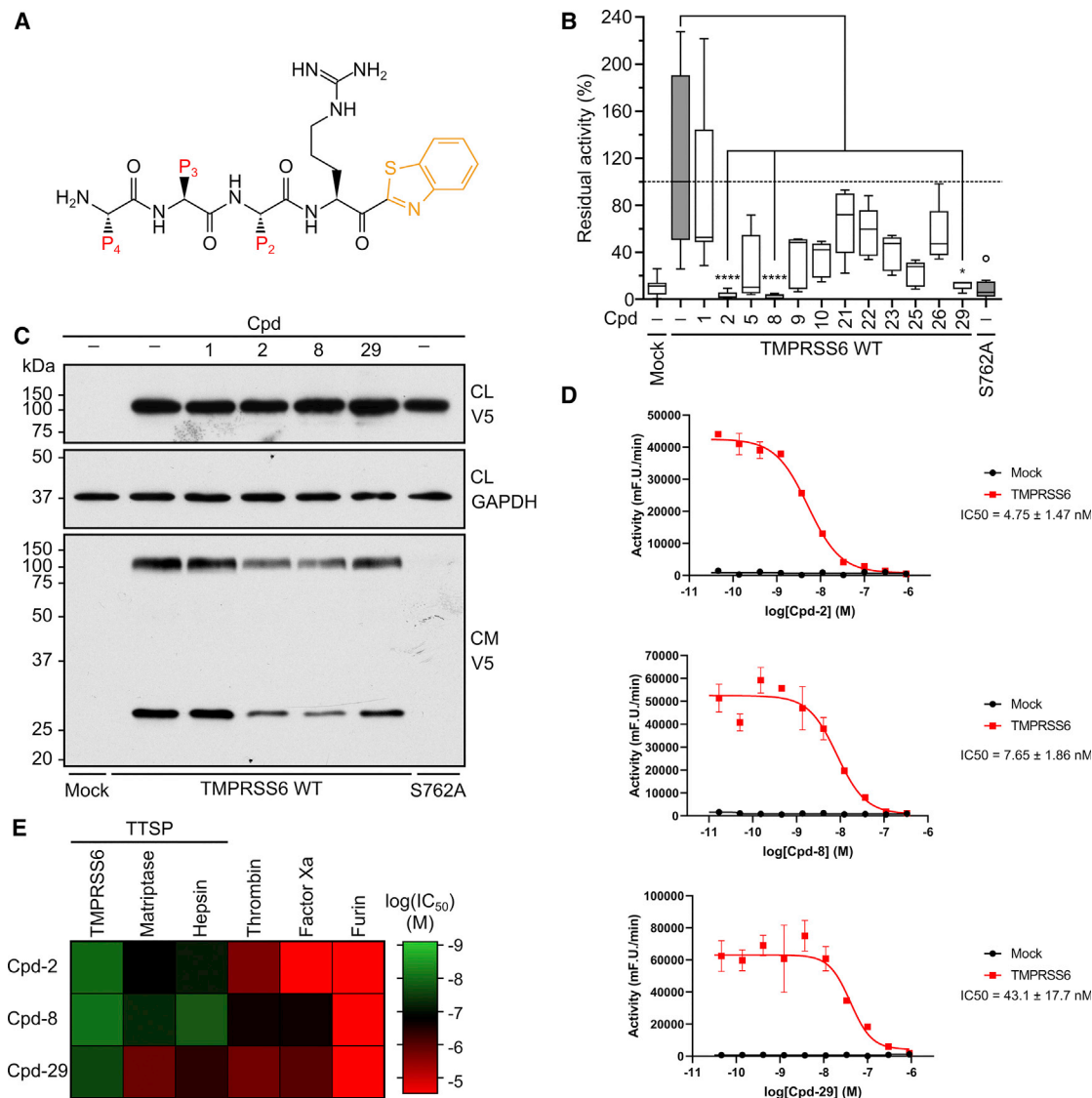


**Figure 1. Inhibition by Benzothiazole-Based Compounds**

(A) Generic scaffold of ketobenzothiazole serine trap peptidomimetic inhibitors. Positions P4, P3, and P2 (red) were varied using natural and unnatural amino acids when position P1 was fixed to Arg. A ketobenzothiazole serine trap is present in the C-terminal position (orange).

(B) HEK293 cells were transfected with TMPRSS6-V5 and cell media were replaced after 24 h with serum-free media with or without inhibitor. Activity in cell media treated or not with 100 nM inhibitor was evaluated 24 h after media change with Boc-QAR-AMC fluorescent substrate and reported as percent residual activity. Boxes show quartiles and whiskers show the last data within 1.5 interquartile range between lower and upper quartile (Tukey boxplot) ( $n \geq 5$ ). Statistical analyses were determined using Kruskal-Wallis test. Asterisks indicate significant differences from TMPRSS6-V5 controls treated with vehicle (0.1% DMSO). \* $p < 0.05$ , \*\*\*\* $p < 0.0001$ .

(C) Immunoblotting of TMPRSS6-V5 in cell lysate (CL) and cell media with reference compound (Cpd-1) and inhibitors (100 nM) exhibiting the highest level of inhibition of proteolytic activity (compounds 2, 8, and 29). Expression was detected by western blotting with anti-V5 antibody. An equal amount of CL was loaded on an SDS-polyacrylamide gel (upper panels). The cell medium (CM) was concentrated and loaded on a 12% SDS-polyacrylamide gel (lower panel). CL GAPDH was blotted as a loading control ( $n = 3$ ) (middle panel).

(D) Mean  $IC_{50}$  values were determined by monitoring proteolytic activity in cell media of HEK293 transfected cells treated with inhibitors significantly decreasing TMPRSS6's activity. Relative activity is expressed as millifluorescence units per minutes (mF.U./min). Mean values  $\pm$  SD are presented alongside a representative  $IC_{50}$  curve.

(E) Specificity of benzothiazole-based compounds toward other serine proteases. Data are represented as a heat map using  $\log(IC_{50})$  mean values,  $N \geq 3$ .

See also [Figures S1–S3](#) and [Tables S1–S3](#).

of thrombin and factor Xa and had no inhibitory activity toward furin.

Overall, compounds showed specificity for TTSPs with a preference for TMPRSS6. Because Cpd-8 is a potent TMPRSS6

inhibitor both *in vitro* and *in cellulo* and is the most stable in mouse plasma compared with Cpd-2 (St-Georges et al., 2017), it was selected for further characterization as a tool compound for its potential effect on BMP6-HJV-hepcidin axis modulation.

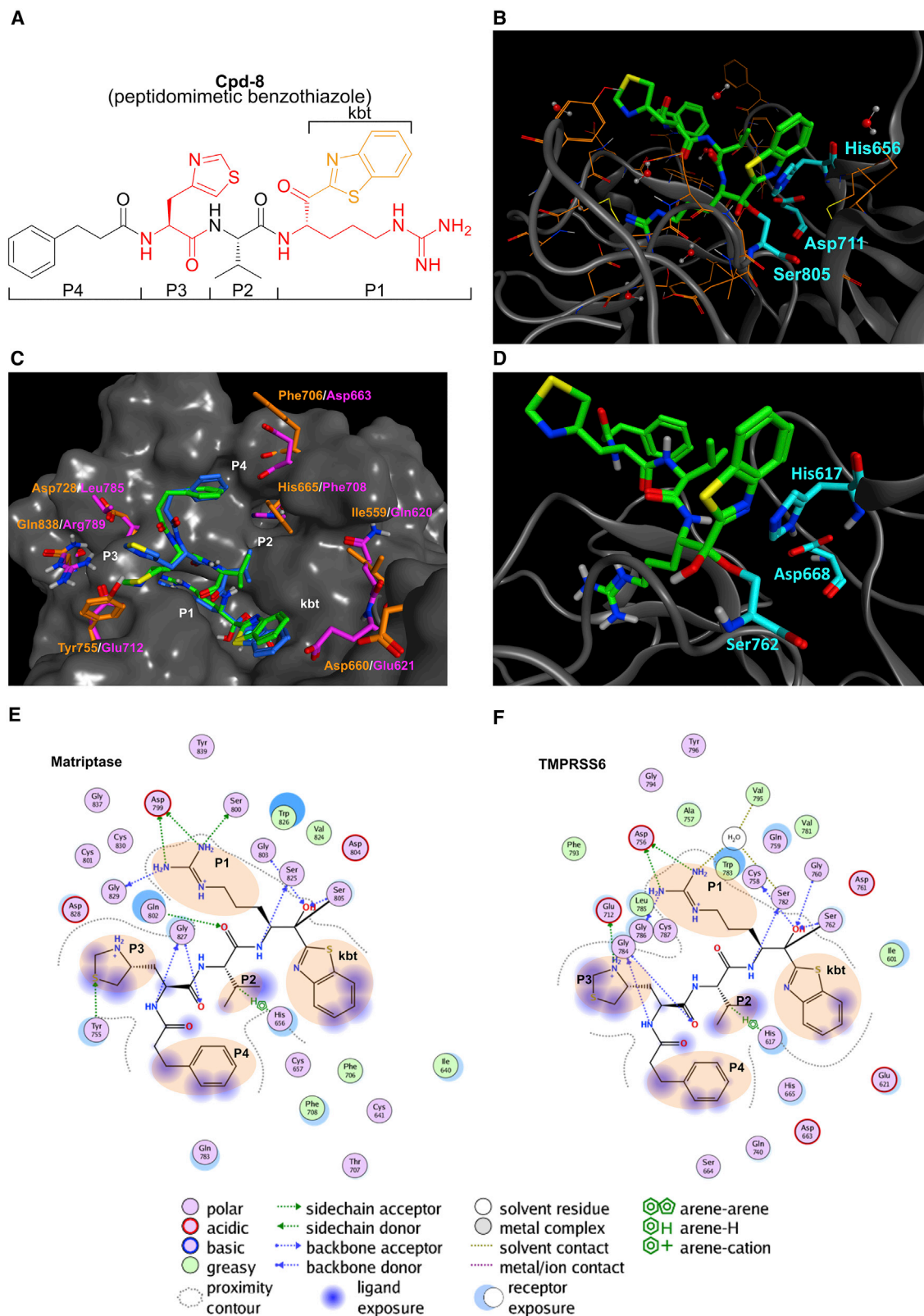


**Figure 2. Interactions of Cpd-8 with Matriptase and TMPRSS6**

(A) Chemical structure of benzothiazole inhibitor Cpd-8. The compound is composed of a desaminophenylalanine residue (P4), (thiazol-4-yl)alanine (P3), valine (P2), arginine (P1), and a ketobenzothiazole (kbt) at the C terminus.

(legend continued on next page)

### Cpd-8 Forms a Reversible Covalent Bond with TMPRSS6

Cpd-8 is composed of a desamino phenylalanine residue in P4, (thiazol-4-yl)alanine in P3, valine in P2, arginine in P1, and a ketobenzothiazole at the C terminus (Figure 2A). To understand how this compound achieves its high inhibitory potential, we obtained a crystal structure of this compound bound to matriptase (PDB: 6N4T; Figure 2B). A homology model of TMPRSS6 was then built using the crystal structure of matriptase (Figure 2C). Alignment to the residues of the catalytic domain of matriptase resulted in 45% and 62% sequence identity and similarity, respectively, allowing to build a high-quality model. We had previously published a homology model of TMPRSS6 (St-Georges et al., 2017) based on a different matriptase crystal (PDB: 3NCL; Brown et al., 2011). Comparison of those TMPRSS6 homology models revealed only two minor differences, mostly due to the shape and the conformation of their corresponding ligand. First, to accommodate the P2 Val residue (PDB: 6N4T), Phe708 side chain must rotate 90°. Finally, translation and rotation of Gln801 allows the formation of a hydrogen bond with the first amide bond of Cpd-8, which was not possible with benzamidine phosphate inhibitors as shown in Figure S4A.

Superimposition of the previously proposed model (docked with inhibitor Y-Y-V-R-Kbt) with the newly obtained crystal structure of matriptase with Cpd-8 (PDB: 6N4T) shows a good overlay of the peptidomimetic backbone of both inhibitors (see Figure S4B). Moreover, no major difference can be observed around the binding pocket of matriptase and TMPRSS6 regarding the orientation of the amino acids for each enzyme. In other words, the new crystal structure did not provide major new insights into the possible future design of molecules or the interpretation of the selectivity of peptides. Comparison of the binding pocket of matriptase and TMPRSS6's homology model revealed only seven differences (Figure 2C). At the P2 position, matriptase His665 is replaced by Phe708 in TMPRSS6, another aromatic residue. There are also three major differences around (thiazol-4-yl)alanine in P3, which can eventually be used to optimize selectivity: Asp728 → Leu785, Gln838 → Arg789, and Tyr755 → Glu712. Along these lines, at the P4 extension, aromatic residue Phe706 is replaced by an acidic and polar Asp663. Another variation is located in the ketobenzothiazole environment while the polar hydrophilic Gln620 replaces the hydrophobic Ile559. Another important difference is a deletion of three residues observed for TMPRSS6 leading to a conformational change and a complete flip of Glu621 which replaces Asp660 in matriptase.

A striking observation is that Cpd-8 forms a covalent bond with the catalytic triad residue Ser762 of TMPRSS6 (His617 and Asp668) as shown in Figure 2D, which is also found in the crystal structure of matriptase (Figure 2B). To the best of our knowledge, this constitutes the first observation of the covalent bond formation of ketobenzothiazoles with TTSPs. This observation strongly supports the designed reversible tight-binding mode of inhibition.

A closer look at the models reveal key interactions inside the binding pocket between Cpd-8 and matriptase (crystal structure) as well as with TMPRSS6 (homology model) (Figures 2E and 2F). A strong hydrogen bond network is observed between the guanidinium group (-C-(NH<sub>2</sub>)<sup>2+</sup>) of Cpd-8 Arg (P1) and Asp799 in matriptase (Figure 2E) or the equivalent Asp756 position in TMPRSS6 (Figure 2F). The guanidinium group was found deep in the catalytic pocket, which is common for this type of enzyme (Czapinska and Otlewski, 1999). Gly829 (matriptase) and Gly786 (TMPRSS6) are the backbone hydrogen bond acceptor in both cases. Another interesting interaction is an arene-H between a proton of the Cpd-8 Val (P2) side chain and His656 (matriptase) or His617 (TMPRSS6), which is part of the catalytic triad. Other similarities include hydrogen bond acceptors and donors of the (thiazol-4-yl)alanine (P3) backbone with Gly827 (matriptase) and Gly784 (TMPRSS6), a hydrogen bond between the arginine (P1) amide and the Ser825 (matriptase) or Ser782 (TMPRSS6) backbone, and a hydrogen bond network with Gly803 and Ser805 (matriptase) or Gly760 and Ser762 (TMPRSS6), which presumably plays a critical role in the hemiketal formation and stability. Ligand exposures are also identical and include a benzothiazole aromatic ring, desamino phenylalanine, and (thiazol-4-yl)alanine.

Conversely, differences were also observed. Matriptase Tyr755 is replaced in TMPRSS6 with a smaller residue (Glu712) leading to a conformation change of the ligand to accommodate the (thiazol-4-yl)alanine in the crystal structure of matriptase. Sulfur forms a hydrogen bond with the phenol group of the tyrosine. However, Glu712 in the TMPRSS6 model plays a similar role and is a side chain hydrogen bond acceptor with the (thiazol-4-yl)alanine amine instead.

### Inhibition of TMPRSS6 by Non-peptidic Compounds

Use of peptidic compounds as drugs is limited by their rapid proteolysis and generally poor membrane permeability and oral bioavailability (Qvit et al., 2017). In an attempt to identify more druggable compounds, an integrated screening approach was used to identify TMPRSS6 inhibitors (Leveridge et al., 2018) in which both a conventional HTS campaign and a DNA-encoded library screen ELT (Arico-Muendel, 2016) were performed. HTS was conducted against GSK's collection of around 2 million compounds, with each compound tested at 10 μM using a fluorescence-based assay for TMPRSS6 activity. The screen output was triaged by re-testing putative hits in dose-response tests conducted under a range of conditions to give preliminary information on potency, specificity (versus matriptase) and inhibition mechanism (e.g., time-dependence of inhibition). Potentially useful chemotypes were then confirmed by re-synthesis of exemplars and re-testing against TMPRSS6. In the case of ELT, selections were performed against purified TMPRSS6 using methods described previously (Arico-Muendel, 2016; Belyanskaya et al., 2017), and putative hits were re-synthesized and tested as described above.

(B) Cpd-8 forms a covalent bond with matriptase catalytic triad residue Ser7805. Residues of the catalytic triad are shown in cyan and Cpd-8 in green.

(C) Comparison of the binding pocket of matriptase crystal structure (PDB: 6N4T) (orange) and TMPRSS6 homology model (purple). Matriptase-associated Cpd-8 is blue and green for TMPRSS6.

(D) Cpd-8 forms a covalent bond with catalytic triad residue Ser762. Residues of the catalytic triad are shown in cyan and Cpd-8 in green.

(E and F) Interactions of Cpd-8 with (E) matriptase and (F) TMPRSS6. Orange highlights inhibitor side chains.

See also Figure S4 and Table S4.

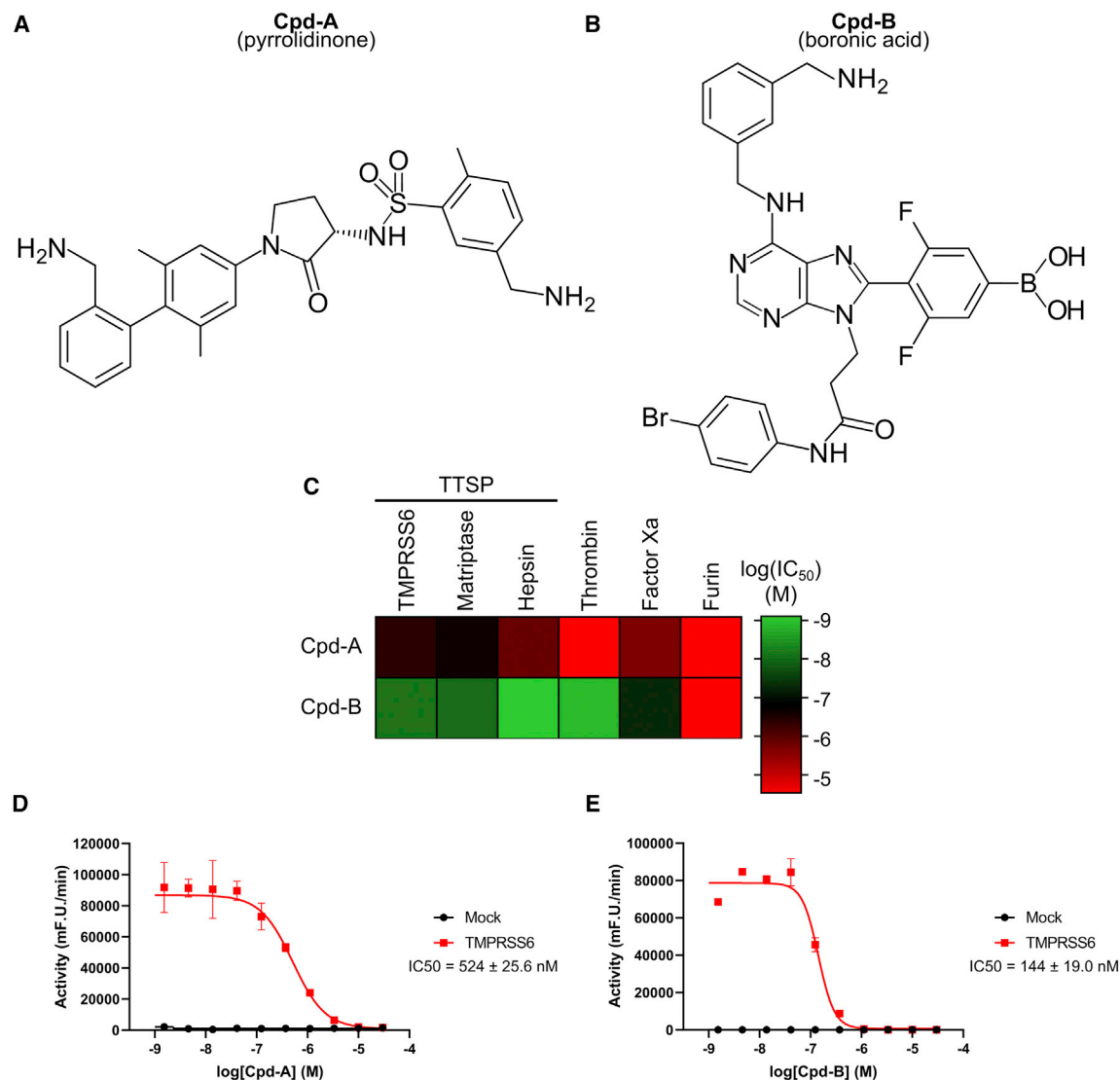


**Figure 3. Inhibition by Non-peptidic Inhibitors Derived from High-Throughput Screening**

(A and B) Chemical structures of Cpd-A (A) and Cpd-B (B).

(C) Specificity of non-peptidic compounds toward TMPRSS6 and other serine proteases. Data are represented as a heatmap using  $\log(\text{IC}_{50})$  mean values,  $N \geq 3$ . (D–E) Mean  $\text{IC}_{50}$  values for Cpd-A (D) and Cpd-B (E) were determined by monitoring proteolytic activity in cell media of HEK293 transfected cells treated with inhibitors significantly decreasing TMPRSS6's activity. Relative activity is expressed as millifluorescence units per minutes (mF.U./min). Mean values  $\pm$  SD are presented along a representative  $\text{IC}_{50}$  curve.

See also Figures S2 and S3 and Table S3.

These screening campaigns led to the identification of chemical templates from two distinct classes, pyrrolidinones and boronic acids, showing a reasonable level of potency and specificity for TMPRSS6. The initial hits were optimized via chemical modification, and both classes of compounds are predicted to inhibit through the binding of the active sites of proteases (work to be published elsewhere).

We selected examples from each of these inhibitor series (Cpd-A, pyrrolidinone; Cpd-B, boronic acid; Figures 3A and 3B) to characterize their effects in cellular systems in comparison with the highly potent peptidomimetic, Cpd-B. Next, we characterized the specificity of compounds *in vitro* (see Figure 3C for heatmap

representation supported by Table S3). When compared with Cpd-B, Cpd-A was shown to be less potent toward TMPRSS6 ( $\text{IC}_{50}$  Cpd-A = 416 nM versus Cpd-B = 7.6 nM). However, it is also weaker toward the other TTSP family members matriptase and hepsin. Furthermore, it is a very weak inhibitor of factor Xa and thrombin, whereas Cpd-B remains highly potent against these proteases. Both compounds showed no activity toward furin. Accordingly, while the pyrrolidinone Cpd-A showed weaker potency against TMPRSS6 compared with the highly potent boronic acid Cpd-B, it possessed higher selectivity.

We then performed *in cellulo*  $\text{IC}_{50}$  measurements for these compounds in cell media of TMPRSS6-transfected HEK293

cells, as for Cpd-8 (Figure 1D). These compounds showed around 2-log difference in  $IC_{50}$  values compared with Cpd-8 with an  $IC_{50}$  of  $524 \pm 26$  nM (Cpd-A; Figure 3D) and  $144 \pm 19$  nM (Cpd-B Figure 3E) and no cytotoxicity was detected at the highest concentration used (30  $\mu$ M) (Figure S2A). Regarding peptidomimetic compounds, Cpd-A and -B did not negatively affect TMPRSS6 plasma membrane localization (Figure S3A). Although less potent than Cpd-8, these inhibitors did appear suitable for testing the effects of TMPRSS6 inhibition in physiologically relevant cellular systems.

### Inhibition of Hemojuvelin Cleavage in HepG2 Cells

To evaluate the inhibitors' efficiency in a cellular context, we assessed their ability to prevent the cleavage of HJV, a TMPRSS6 substrate found at the apex of the BMP/SMAD signaling pathway, in co-transfected HepG2 cells known to express hepcidin endogenously (Dion et al., 2018b; Fein et al., 2007; Gehrke, 2003; Kulaksiz, 2004). TMPRSS6 cleaves HJV at two different sites, C-terminal to Arg121 and Arg326, leading to the production of fragments of various lengths that are released in the cell medium (Rausa et al., 2015). In our assay, cells were first co-transfected with TMPRSS6-V5 and HJV for 24 h before being incubated in the presence of increasing concentrations of compounds for another 24 h.  $IC_{50}$  values for inhibition of HJV cleavage *in cellulo* were calculated by densitometry quantification from an HJV signal originating from western blot analysis of cell-released immune-reactive soluble fragments found in the media (Figures 4A–4C). In this system, the rank order of potency of the inhibitors was maintained (Cpd-8 > Cpd-B > Cpd-A), but with approximately a 2- to 10-fold loss of potency compared with inhibition of shed TMPRSS6 activity. Of note, the highest concentration of compounds used (10  $\mu$ M) has no cytotoxic effect in those cells (Figure S2B). Furthermore, compounds did not negatively affect the cell surface expression of TMPRSS6 or HJV, indicating that their mechanism of action involves inhibition of protease activity preventing cell surface shedding (Figures S3B and S3C). These results provide evidence that inhibiting TMPRSS6 proteolytic activity prevents cleavage of HJV, and that all three exemplar inhibitors had the potential to modulate BMP/hepcidin signaling at relatively low doses.

### TMPRSS6 Inhibition Increases HAMP Expression

To further determine the impact of inhibitors on the hepcidin pathway, we evaluated their effects on hepcidin encoding gene (*HAMP*) expression by using a BacMam transduction system to express increasing amounts of TMPRSS6 in HepG2 cells and by evaluating *HAMP* transcript levels by qRT-PCR. In accordance with previous results (Silvestri et al., 2008a), increasing the expression levels of TMPRSS6 led to a decrease of *HAMP* in our model (Figure 5A). To validate whether the observed effects were due to the catalytic activity of TMPRSS6, we compared *HAMP* levels in HepG2 cells transduced with the same amount of TMPRSS6 (1%), with either the wild-type (TMPRSS6-WT) or the catalytically inactive enzyme (TMPRSS6-S762A; Figures 5B and S5 for western blot analysis of transduced TMPRSS6). This comparison confirmed a strong reduction in *HAMP* expression with TMPRSS6-WT but a much lower (although measurable) reduction with TMPRSS6-S762A (Figure 5B). We have shown previously that TMPRSS6-S762A can still interact

with HJV, despite its inactivity (Dion et al., 2018b). Suggesting that TMPRSS6-S762A's effect on *HAMP* could be the result of an interaction with one of its substrates, independently of cleavage. Nonetheless, these data confirm that TMPRSS6 catalytic activity plays a significant role in *HAMP* modulation in this model, and that TMPRSS6 inhibitors may have efficacy in modulating *HAMP*.

HepG2 cells were then transduced with TMPRSS6-WT (1%) and incubated with vehicle (0.1% DMSO) and inhibitors at concentrations ranging from 0.1 to 10  $\mu$ M (Figures 5C–5E). All classes of compounds (doses of 1 and 10  $\mu$ M for Cpd-8 and Cpd-B and 10  $\mu$ M for Cpd-A), significantly increased *HAMP* levels (Figures 5C–5E). Furthermore, *HAMP* fold changes observed are in line to those found for hepcidin, as determined by ELISA, when cells were treated with compound concentration of 1  $\mu$ M (Figure 5F). As a control, experiments were performed with TMPRSS6-S762A-transduced cells and no *HAMP* increase was observed (Figure S6). Overall, these results show that all three classes of compound can increase *HAMP* and hepcidin by inhibiting TMPRSS6 activity in a heterologous expression system.

### TMPRSS6 Inhibition Increases Hepcidin Expression in Human Primary Hepatocytes

To validate the effects of the compounds on hepcidin expression in a more physiologically relevant model, we used human primary hepatocytes originating from four different donors. Hepatocytes were treated with vehicle (0.1% DMSO) or increasing concentrations (0.1, 1, 5, and 10  $\mu$ M) of inhibitors (Figures 6A–6C). After a 6-h treatment, cells were stimulated with hBMP6 for 24 h before *HAMP* expression analysis in cellular extracts. Cpd-8 displayed a dose-dependent increase in *HAMP* expression with maximum fold change (4.1) over untreated cells (Figure 6A). Only the 10  $\mu$ M concentration yielded a significantly different fold change for the four donors ( $p < 0.05$ ), but a general increasing trend was observed for all concentrations. Similar results were obtained for Cpd-A (maximum fold change at 2.7) and Cpd-B (maximum fold change at 4.4). To support these data, we analyzed the additional BMP/SMAD target genes *ID1*, *SMAD7*, and *TMPRSS6* (Meynard et al., 2011) under the same conditions and detected an increase in *ID1* at 10  $\mu$ M for all three compounds (Figure S7). While we observed a general trend, no statistically significant differences were observed with both *SMAD7* and *TMPRSS6* (Figure S7). To verify if increased *HAMP* expression also increased hepcidin levels, we analyzed the levels of hepcidin in the cell media by ELISA for one of the donors (8279; Figure 7). All three compounds showed a dose-dependent increase of hepcidin, although only Cpd-8 and Cpd-A led to a significantly higher levels of 5 and 10  $\mu$ M (Figures 7A and 7B). Importantly, no cytotoxicity was detected for the three compounds at the highest used concentration (10  $\mu$ M) (Figure S2C). Collectively, these results demonstrate that all three classes of TMPRSS6 inhibitors modulate *HAMP*/hepcidin expression in human primary hepatocytes, but likely will require further optimization to be useful *in vivo*.

### DISCUSSION

TMPRSS6 is a key component of iron homeostasis through its regulation of hepcidin, a 25-amino acid peptide liver

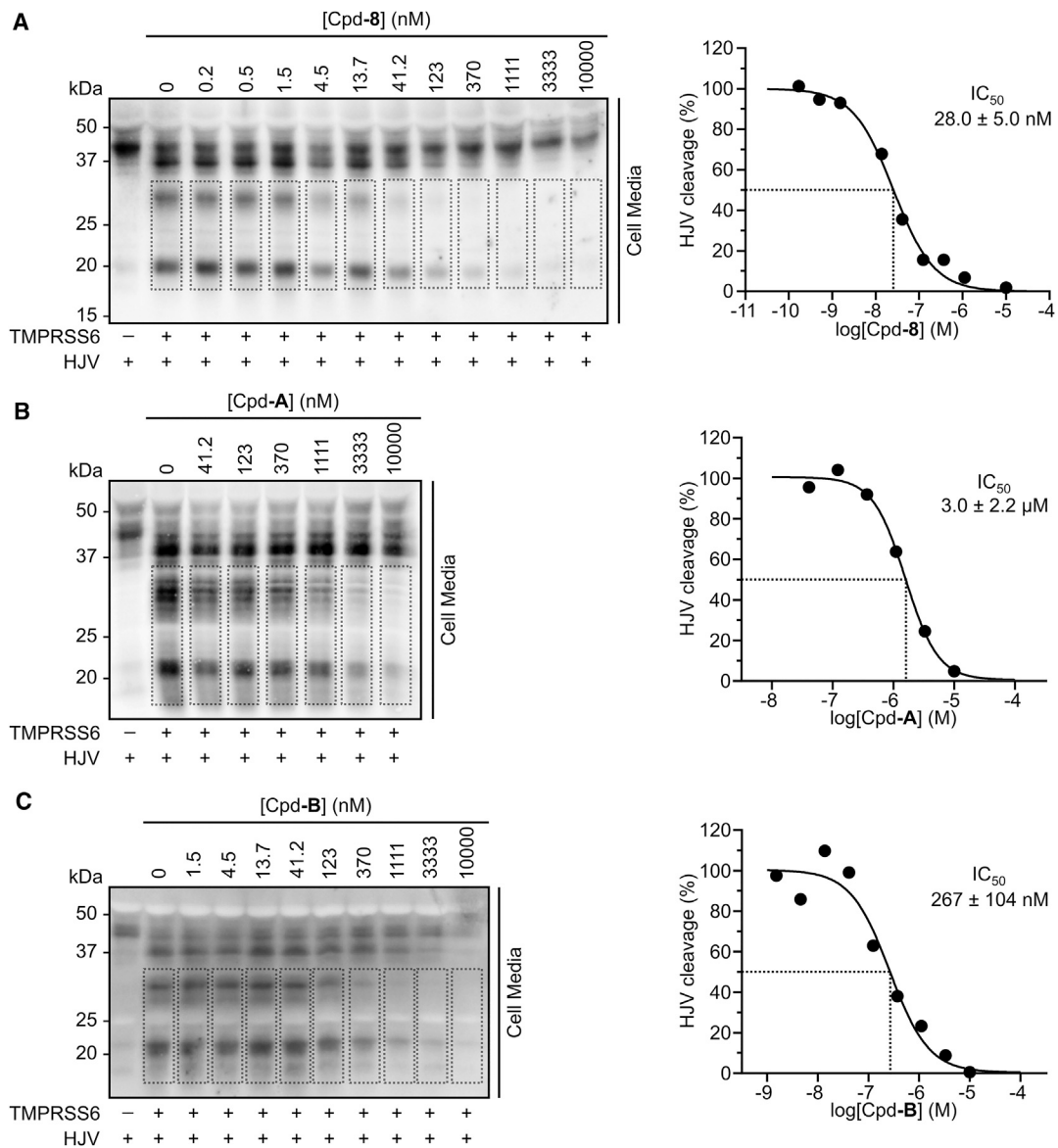


**Figure 4. Inhibition of HJV Cleavage in HepG2 Cells**

HepG2 cells were co-transfected with TMPRSS6-V5 and HJV. Twenty-four hours post transfection, cell media were replaced with serum-free media with (A) Cpd-8, (B) Cpd-A, or (C) Cpd-B concentrations ranging from 0.2 nM up to 10  $\mu$ M for another 24 h. The cell media were concentrated and loaded on a 12% SDS-polyacrylamide gel (n = 3). HJV cleavage was detected by western blotting with anti-HJV antibody. HJV cleavage was quantified by densitometry (dashed rectangles, left panels) and plotted on a graph for  $IC_{50}$  values calculation (right panels). Results are expressed as HJV cleavage (%) relative to vehicle-treated cells (0.1 % DMSO). Mean values  $\pm$  SD are presented for  $IC_{50}$  values (n  $\geq$  3) alongside a representative western blot and  $IC_{50}$  curve. See also [Figures S2](#) and [S3](#).

hormone and master regulator of iron metabolism (Du et al., 2008; Finberg et al., 2008; Ganz and Nemeth, 2012). Impairment of TMPRSS6 functionality, either through the loss of proteolytic activity or reduction of cell surface localization, is associated with low body iron levels and has been found in patients with IRIDA, who have high circulating levels of hepcidin. On the other hand, patients suffering from iron overload disorders have high levels of body iron that are linked to lower hepcidin status. Increasing hepcidin levels could be an attractive therapeutic approach to address conditions of iron overload. For this purpose, several groups have

developed hepcidin agonists using different strategies: hepcidin mimics with FPN as a target; inhibition of FPN or stimulation of hepcidin production by targeting TMPRSS6 (Casu et al., 2018). Published strategies centered around TMPRSS6 have focused on targeting mRNA degradation either by use of ASO (Guo et al., 2013) or small interfering RNA (Schmidt et al., 2013). In mouse models of  $\beta$ -thalassemia intermedia and hereditary hemochromatosis, silencing of *TMPRSS6* led to increased hepcidin levels and reduced serum and liver iron concentration (Casu et al., 2018). However, until now, TMPRSS6 protease inhibitors targeting the enzyme's catalytic

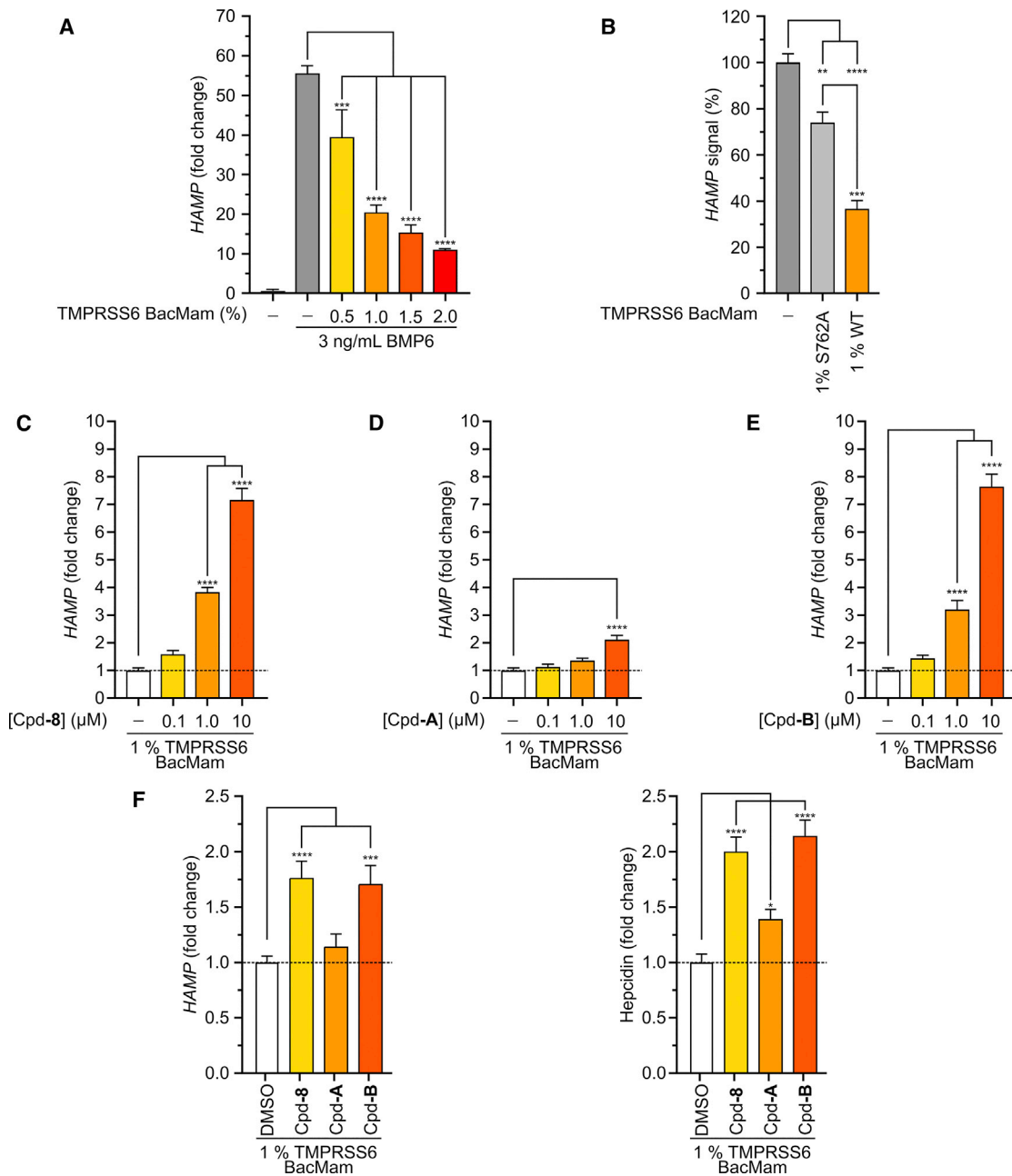


**Figure 5. TMPRSS6 Inhibition Increases *HAMP* Expression in HepG2 Cells**

(A) HepG2 cells were transduced with increasing TMPRSS6 BacMam viral dose (0.5%, 1%, 1.5%, and 2%) and were treated or not with 3 ng/mL hBMP6. *HAMP* expression was quantified by RT-qPCR and expressed as fold change over untransduced (TMPRSS6-WT) and untreated (hBMP6) cells (n = 3).

(B) HepG2 cells were transduced with TMPRSS6-WT or TMPRSS6-S762A (1%) and treated with 3 ng/mL hBMP6. *HAMP* transcripts were quantified by qRT-PCR and expressed as a percentage of untransduced cells *HAMP* signal (*HAMP* signal [%]) (n = 3).

(C–E) HepG2 cells were transduced with TMPRSS6-WT (1%), stimulated with 3 ng/mL hBMP6 and treated with DMSO (0.1%) or increasing Cpd-8 (C), Cpd-A (D), and Cpd-B (E) concentrations (0.1, 1, or 10 μM). *HAMP* expression was quantified by RT-qPCR and expressed as *HAMP* fold change over vehicle-treated cells (DMSO 0.1%) (n = 3).

(F) HepG2 cells were transduced with TMPRSS6-WT (1%), stimulated with 3 ng/mL hBMP6, and treated with vehicle (DMSO 0.1%) or 1 μM compound. *HAMP* expression was quantified by qRT-PCR (left panel) and hepcidin-25 protein in cell media was quantified by ELISA (right panel). Results are expressed as *HAMP* or hepcidin fold change over vehicle-treated cells (n = 3). All statistical analyses were determined using one-way ANOVA. Asterisks indicate significant differences compared with vehicle (DMSO 0.1%)-treated cells. \*p ≤ 0.05, \*\*p ≤ 0.01, \*\*\*p ≤ 0.001; \*\*\*\*p ≤ 0.0001.

See also [Figures S2, S5, and S6](#).

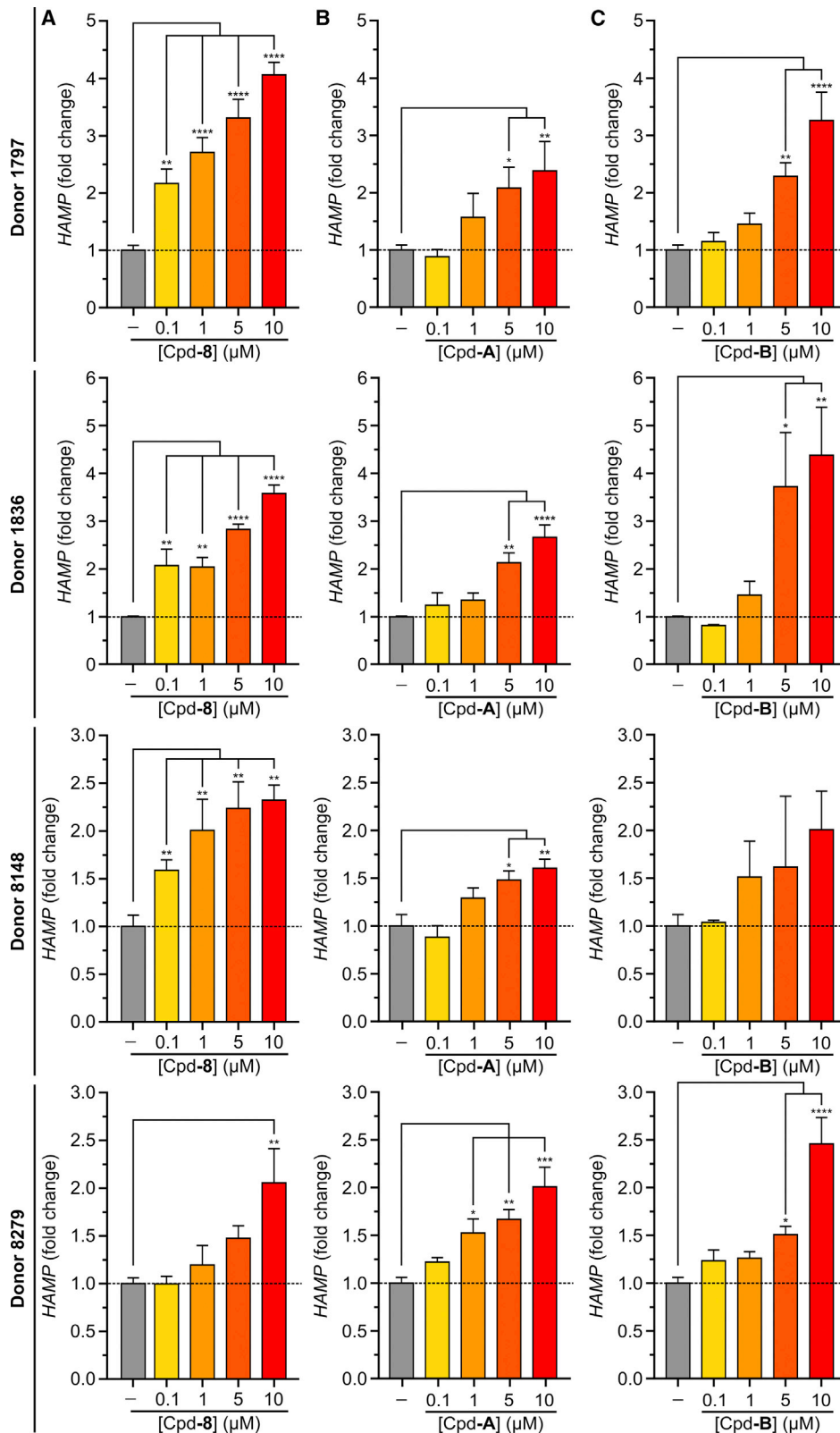


**Figure 6. TMPRSS6 Inhibition Increases HAMP Expression in Human Primary Hepatocytes**

Human primary hepatocytes from four different donors (1797, 1836, 8148, and 8279) were treated with either DMSO (0.1%) or increasing concentrations (0.1, 1, 5, and 10 μM) of (A) Cpd-8, (B) Cpd-A, or (C) Cpd-B at 30 ng/mL hBMP6. Cells were plated in media with fetal bovine serum for 24 h then media (legend continued on next page)

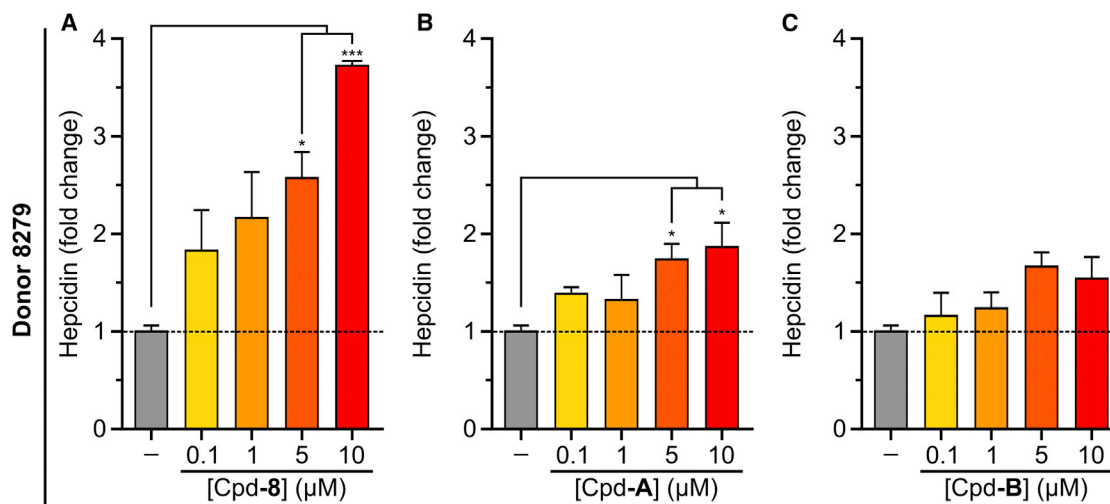


**Figure 7. TMPRSS6 Inhibition Increases Hepcidin Levels in Human Primary Hepatocytes**

Human primary hepatocytes from donor 8279 were treated with either DMSO (0.1%) or increasing concentrations of (A) Cpd-8, (B) Cpd-A, or (C) Cpd-B (0.1, 1, 5, and 10  $\mu$ M) at 5 ng/mL hBMP6. Cells were plated in media with fetal bovine serum for 24 h then media were replaced by serum-free media containing inhibitors for 6 h. hBMP6 was then added for 24 h and hepcidin-25 in cell media was quantified by ELISA. Results are expressed as hepcidin fold change over vehicle-treated cells ( $n = 3$ ). All statistical analyses were determined using one-way ANOVA. Asterisks indicate significant differences compared with vehicle (DMSO 0.1%) treated cells. \* $p < 0.05$ , \*\*\* $p < 0.001$ . See also Figure S2.

activity have not been reported to efficiently modulate hepcidin expression in cellular models.

Data presented herein demonstrate that three different compound classes inhibit TMPRSS6 proteolytic activity in a cellular context. We show that TMPRSS6 inhibition abolishes HJV cleavage, a TMPRSS6 substrate and an upstream element of the BMP/SMAD pathway, leading to the production of hepcidin. These compounds exhibited a dose-dependent increase in *HAMP* expression and hepcidin levels in liver-related models such as HepG2 cells and human primary hepatocytes. Although we cannot rule out the possibility that the effect observed on *HAMP* and hepcidin levels in primary hepatocytes is due to inhibition of off-target proteases, we believe it is likely to be the consequence of TMPRSS6 inhibition. Compounds tested in this study are also potent against matriptase and hepsin (Figures 1E and 3E), two TTSPs with high similarity regarding their catalytic domain when compared with TMPRSS6. However, while matriptase is virtually not expressed in the liver (Table S2), no reported data support the involvement of the liver-expressed hepsin in hepcidin regulation. Refinement of inhibitor selectivity using structure-activity relationship strategy and the use of TMPRSS6 and hepsin knockout hepatocytes would be useful to determine precisely the mechanism of action of these molecules and avoid potential off-target effects. These results could also be very important for further characterization of *in vivo* mouse models of  $\beta$ -thalassemia and hemochromatosis. Overall, compound optimization for the three classes used here (peptidomimetic benzothiazole-based, boronic acids,

and pyrrolidinones) constitute a potential strategy for future studies aimed at developing molecules for therapeutic purposes.

Other groups have developed TMPRSS6 proteolytic inhibitors using different strategies based on benzamide (Sisay et al., 2010), bisbenzamidines (Beckmann et al., 2016b), sunflower trypsin inhibitor-1 (Gitlin et al., 2015; Gitlin-Domagalska et al., 2017), or Kunitz-type inhibitors such as HAI-1 and HAI-2 (Beckmann et al., 2016a). Although some of these exhibit potency and selectivity for TMPRSS6, their use in a cellular context has not been reported. In this study, we demonstrate for the first time that targeting TMPRSS6 proteolytic activity with protease inhibitors can be used to increase hepcidin expression in liver cellular models, constituting a potential therapeutic approach aimed at treating patients with iron overload conditions.

## SIGNIFICANCE

**TMPRSS6 is a key modulator of the iron homeostasis pathway. Previous studies have shown that downregulation of the protease increases hepcidin levels thus reducing iron import. Those studies have also shown that, in models of iron overload diseases, such as hemochromatosis and  $\beta$ -thalassemia, knockout of the enzyme diminishes related effects. However, inhibition of the catalytic activity of the enzyme by small molecules resulting in similar outcomes has not been demonstrated. Here we show that three different classes of proteolytic inhibitors targeting**

were replaced by serum-free media containing inhibitors for 6 h. hBMP6 was then added for 24 h. *HAMP* expression was quantified by RT-qPCR and expressed as *HAMP* fold change over vehicle-treated cells (DMSO 0.1%) ( $n \geq 3$ ). All statistical analyses were determined using one-way ANOVA. Asterisks indicate significant differences compared with vehicle (DMSO 0.1%)-treated cells. \* $p < 0.05$ , \*\* $p < 0.01$ , \*\*\* $p < 0.001$ , \*\*\*\* $p < 0.0001$ . See also Figures S2 and S7.

## TMPRSS6 catalytic activity increase hepcidin production in a liver cellular model and in primary human hepatocytes.

### STAR★METHODS

Detailed methods are provided in the online version of this paper and include the following:

- **KEY RESOURCES TABLE**
- **LEAD CONTACT AND MATERIALS AVAILABILITY**
- **EXPERIMENTAL MODEL AND SUBJECT DETAILS**
  - Chemical Synthesis of Compounds
  - Cell Culture
- **METHOD DETAILS**
  - Screening of Inhibitory Potency in Cells
  - Compounds IC<sub>50</sub> on TMRSS6 Activity *In Cellulo*
  - *In Vitro* IC<sub>50</sub> Determination
  - Compound Toxicity *In Cellulo*
  - Compound Effect on Cell Surface Expression in HEK293 Cells
  - Compound Effect on Cell Surface Expression in HepG2 Cells
  - Matriptase/Cpd-8 Crystal Structure
  - TMPRSS6 Homology Model Using MOE Modeling
  - Hemojuvelin Cleavage Assay
  - TMPRSS6 Western Blot
  - HAMP RT-qPCR
  - Hepsidin Quantification by ELISA
  - *ID1*, *SMAD7* and *TMPRSS6* RT-qPCR
  - Statistical Analysis
- **DATA AND CODE AVAILABILITY**

### SUPPLEMENTAL INFORMATION

Supplemental Information can be found online at <https://doi.org/10.1016/j.chembiol.2019.09.004>.

### ACKNOWLEDGMENTS

This work was supported by the Canadian Institutes of Health Research (CIHR) (grant number MOP 133400) to R.L. and E.M. and by the Discovery Partnerships with Academia (DPAC) group, part of GlaxoSmithKline Research and Development. F.B. has received a MITACS fellowship in partnership with GlaxoSmithKline. S.P.D. is a Ph.D. fellow of the Fonds de Recherche du Québec – Santé (FRQ-S).

### AUTHOR CONTRIBUTIONS

C.St.G. produced and C.St.G., P.-L.B., and E.M. designed the benzothiazole inhibitors. D.P. and J.C. designed Cpd-A and Cpd-B. S.P.D. performed benzothiazole-based compounds screening, IC<sub>50</sub> determination, cell surface localization assays in HEK293 cells, and cytotoxic assays in all cellular models. A.D. performed the compounds IC<sub>50</sub> determination *in vitro*. N.C. determined the crystal structure of Cpd-8 interaction with matriptase. P.-L.B. performed modeling of Cpd-8 in the TMPRSS6 homology model based on matriptase. M.G.G. performed the HJV cleavage assay in HepG2 cells. A.T. performed BacMam assay in HepG2 cells. A.T. and A.G. performed HAMP RT-qPCR assay in human primary hepatocytes. F.B. performed hepcidin ELISA assay in human primary hepatocytes and cell surface localization assays in HepG2 cells. F.B., S.P.D., A.D., P.-L.B., A.J.P., and R.L. wrote the manuscript. R.L. obtained funding from the GSK's Discovery Partnerships with Academia (DPAC) program. All the co-authors reviewed the manuscript.

### DECLARATION OF INTERESTS

R.L. and E.M. hold patent WO2012162828A1 related to peptidomimetic serine protease inhibitors.

Received: November 29, 2018

Revised: June 6, 2019

Accepted: September 3, 2019

Published: September 19, 2019

### REFERENCES

- Adams, P.D., Grosse-Kunstleve, R.W., Hung, L.W., Ioerger, T.R., McCoy, A.J., Moriarty, N.W., Read, R.J., Sacchettini, J.C., Sauter, N.K., and Terwilliger, T.C. (2002). PHENIX: building new software for automated crystallographic structure determination. *Acta Crystallogr. D Biol. Crystallogr.* **58**, 1948–1954.
- Adams, P.D., Afonine, P.V., Bunkóczi, G., Chen, V.B., Davis, I.W., Echols, N., Headd, J.J., Hung, L.-W., Kapral, G.J., Grosse-Kunstleve, R.W., et al. (2010). PHENIX: a comprehensive Python-based system for macromolecular structure solution. *Acta Crystallogr. D Biol. Crystallogr.* **66**, 213–221.
- Antalis, T.M., Bugge, T.H., and Wu, Q. (2011). Membrane-anchored serine proteases in health and disease. *Prog. Mol. Biol. Transl. Sci.* **99**, 1–50.
- Arico-Muendel, C.C. (2016). From haystack to needle: finding value with DNA encoded library technology at GSK. *MedChemComm* **7**, 1898–1909.
- Aschemeyer, S., Qiao, B., Stefanova, D., Valore, E.V., Sek, A.C., Ruwe, T.A., Vieth, K.R., Jung, G., Casu, C., Rivella, S., et al. (2018). Structure-function analysis of ferroportin defines the binding site and an alternative mechanism of action of hepcidin. *Blood* **131**, 899–910.
- Barré, O., Dufour, A., Eckhard, U., Kappelhoff, R., Béliveau, F., Leduc, R., and Overall, C.M. (2014). Cleavage specificity analysis of six type II transmembrane serine proteases (TTSPs) using PICS with proteome-derived peptide libraries. *PLoS One* **9**, 7–11.
- Beckmann, A.M., Maurer, E., Lültsdorf, V., Wilms, A., Furtmann, N., Bajorath, J., Gütschow, M., and Stirnberg, M. (2016a). En route to new therapeutic options for iron overload diseases: matriptase-2 as a target for Kunitz-type inhibitors. *ChemBioChem* **17**, 595–604.
- Beckmann, A.M., Gilberg, E., Gattner, S., Huang, T.L., Vanden Eynde, J.J., Mayence, A., Bajorath, J., Stirnberg, M., and Gütschow, M. (2016b). Evaluation of bisbenzamidines as inhibitors for matriptase-2. *Bioorg. Med. Chem. Lett.* **26**, 3741–3745.
- Béliveau, F., Désilets, A., and Leduc, R. (2009). Probing the substrate specificities of matriptase, matriptase-2, hepsin and DESC1 with internally quenched fluorescent peptides. *FEBS J.* **276**, 2213–2226.
- Béliveau, F., Brulé, C., Désilets, A., Zimmerman, B., Laporte, S.A., Lavoie, C.L., and Leduc, R. (2011). Essential role of endocytosis of the type II transmembrane serine protease TMPRSS6 in regulating its functionality. *J. Biol. Chem.* **286**, 29035–29043.
- Belyanskaya, S.L., Ding, Y., Callahan, J.F., Lazaar, A.L., and Israel, D.I. (2017). Discovering drugs with DNA-encoded library technology: from concept to clinic with an inhibitor of soluble epoxide hydrolase. *ChemBioChem* **18**, 837–842.
- Brosseau, J.-P., Lucier, J.-F., Lapointe, E., Durand, M., Gendron, D., Gervais-Bird, J., Tremblay, K., Perreault, J.-P., and Elela, S.A. (2010). High-throughput quantification of splicing isoforms. *RNA* **16**, 442–449.
- Brown, C.M., Ray, M., Eroy-Reveles, A.A., Egea, P., Tajon, C., and Craik, C.S. (2011). Peptide length and leaving-group sterics influence potency of peptide phosphonate protease inhibitors. *Chem. Biol.* **18**, 48–57.
- Buzza, M.S., Netzel-Arnett, S., Shea-Donohue, T., Zhao, A., Lin, C.-Y., List, K., Szabo, R., Fasano, A., Bugge, T.H., and Antalis, T.M. (2010). Membrane-anchored serine protease matriptase regulates epithelial barrier formation and permeability in the intestine. *Proc. Natl. Acad. Sci. U S A* **107**, 4200–4205.
- Casu, C., Aghajani, M., Oikonomidou, P.R., Guo, S., Monia, B.P., and Rivella, S. (2016). Combination of Tmprss6-ASO and the iron chelator deferiprone improves erythropoiesis and reduces iron overload in a mouse model of beta-thalassemia intermedia. *Haematologica* **101**, e8–e11.

- Casu, C., Nemeth, E., and Rivella, S. (2018). Hcpicidin agonists as therapeutic tools. *Blood* *131*, 1790–1794.
- Corbeil, C.R., Williams, C.I., and Labute, P. (2012). Variability in docking success rates due to dataset preparation. *J. Comput. Aided Mol. Des.* *26*, 775–786.
- Czapinska, H., and Otlewski, J. (1999). Structural and energetic determinants of the S1-site specificity in serine proteases. *Eur. J. Biochem.* *260*, 571–595.
- Dion, S.P., Béliveau, F., Désilets, A., Ghinet, M.G., and Leduc, R. (2018a). Transcriptome analysis reveals TMPRSS6 isoforms with distinct functionalities. *J. Cell. Mol. Med.* *22*, 2498–2509.
- Dion, S.P., Béliveau, F., Morency, L.-P., Désilets, A., Najmanovich, R., and Leduc, R. (2018b). Functional diversity of TMPRSS6 isoforms and variants expressed in hepatocellular carcinoma cell lines. *Sci. Rep.* *8*, 12562.
- Dosa, S., Stirnberg, M., Lültsdorff, V., Häußler, D., Maurer, E., and Gütschow, M. (2012). Active site mapping of trypsin, thrombin and matriptase-2 by sulfamoyl benzamidines. *Bioorg. Med. Chem.* *20*, 6489–6505.
- Du, X., She, E., Gelbart, T., Truksa, J., Lee, P., Xia, Y., Khovananth, K., Mudd, S., Mann, N., Moresco, E.M.Y., et al. (2008). The serine protease TMPRSS6 is required to sense iron deficiency. *Science* *320*, 1088–1092.
- Duchêne, D., Colombo, E., Désilets, A., Boudreault, P.L., Leduc, R., Marsault, E., and Najmanovich, R. (2014). Analysis of subpocket selectivity and identification of potent selective inhibitors for matriptase and matriptase-2. *J. Med. Chem.* *57*, 10198–10204.
- Emsley, P., and Cowtan, K. (2004). Coot: model-building tools for molecular graphics. *Acta Crystallogr. D Biol. Crystallogr.* *60*, 2126–2132.
- Fein, E., Merle, U., Ehehalt, R., Herrmann, T., and Kulaksiz, H. (2007). Regulation of hepcidin in HepG2 and RINm5F cells. *Peptides* *28*, 951–957.
- Finberg, K.E., Heeney, M.M., Campagna, D.R., Aydinok, Y., Pearson, H.A., Hartman, K.R., Mayo, M.M., Samuel, S.M., Strouse, J.J., Markianos, K., et al. (2008). Mutations in TMPRSS6 cause iron-refractory iron deficiency anemia (IRIDA). *Nat. Genet.* *40*, 569–571.
- Finberg, K.E., Whittlesey, R.L., Fleming, M.D., and Andrews, N.C. (2010). Down-regulation of Bmp/Smad signaling by Tmprss6 is required for maintenance of systemic iron homeostasis. *Blood* *115*, 3817–3826.
- Finberg, K.E., Whittlesey, R.L., and Andrews, N.C. (2011). Tmprss6 is a genetic modifier of the Hfe-hemochromatosis phenotype in mice. *Blood* *117*, 4590–4599.
- Folgueras, A.R., de Lara, F.M., Pendás, A.M., Garabaya, C., Rodríguez, F., Astudillo, A., Bernal, T., Cabanillas, R., López-Otín, C., and Velasco, G. (2008). Membrane-bound serine protease matriptase-2 (Tmprss6) is an essential regulator of iron homeostasis. *Blood* *112*, 2539–2545.
- Ganz, T., and Nemeth, E. (2012). Hcpicidin and iron homeostasis. *Biochim. Biophys. Acta* *1823*, 1434–1443.
- Gehrke, S.G. (2003). Expression of hepcidin in hereditary hemochromatosis: evidence for a regulation in response to the serum transferrin saturation and to non-transferrin-bound iron. *Blood* *102*, 371–376.
- Gitlin, A., Dębowski, D., Karna, N., Łęgowska, A., Stirnberg, M., Gütschow, M., and Rolka, K. (2015). Inhibitors of matriptase-2 based on the trypsin inhibitor SFTI-1. *ChemBioChem* *16*, 1601–1607.
- Gitlin-Domagalska, A., Dębowski, D., Łęgowska, A., Stirnberg, M., Okońska, J., Gütschow, M., and Rolka, K. (2017). Design and chemical syntheses of potent matriptase-2 inhibitors based on trypsin inhibitor SFTI-1 isolated from sunflower seeds. *Biopolymers* *108*, <https://doi.org/10.1002/bip.23031>.
- Goswami, R., Mukherjee, S., Wohlfahrt, G., Ghadiyaram, C., Nagaraj, J., Chandra, B.R., Sistla, R.K., Satyam, L.K., Samiulla, D.S., Moilanen, A., et al. (2013). Discovery of pyridyl bis(oxy)dibenzimidamide derivatives as selective matriptase inhibitors. *ACS Med. Chem. Lett.* *4*, 1152–1157.
- Guo, S., Casu, C., Gardenghi, S., Booten, S., Aghajan, M., Peralta, R., Watt, A., Freier, S., Monia, B.P., and Rivella, S. (2013). Reducing TMPRSS6 ameliorates hemochromatosis and  $\beta$ -thalassemia in mice. *J. Clin. Invest.* *123*, 1531–1541.
- Häußler, D., Mangold, M., Furtmann, N., Braune, A., Blaut, M., Bajorath, J., Stirnberg, M., and Gütschow, M. (2016). Phosphono bisbenzguanidines as irreversible dipeptidomimetic inhibitors and activity-based probes of matriptase-2. *Chemistry* *22*, 8525–8535.
- Hellemans, J., Mortier, G., De Paepe, A., Speleman, F., and Vandesompele, J. (2007). qBase relative quantification framework and software for management and automated analysis of real-time quantitative PCR data. *Genome Biol.* *8*, R19.
- Hooper, J.D., Clements, J.A., Quigley, J.P., and Antalis, T.M. (2001). Type II transmembrane serine proteases. Insights into an emerging class of cell surface proteolytic enzymes. *J. Biol. Chem.* *276*, 857–860.
- Kulaksiz, H. (2004). Pro-hepcidin: expression and cell specific localisation in the liver and its regulation in hereditary haemochromatosis, chronic renal insufficiency, and renal anaemia. *Gut* *53*, 735–743.
- Leveridge, M., Chung, C.-W., Gross, J.W., Phelps, C.B., and Green, D. (2018). Integration of lead discovery tactics and the evolution of the lead discovery toolbox. *SLAS Discov.* *23*, 881–897.
- Liu, J., Liu, W., Liu, Y., Miao, Y., Guo, Y., Song, H., Wang, F., Zhou, H., Ganz, T., Yan, B., et al. (2019). New thiazolidinones reduce iron overload in mouse models of hereditary hemochromatosis and  $\beta$ -thalassemia. *Haematologica* *104*, 1768–1781.
- Maurer, E., Gütschow, M., and Stirnberg, M. (2013). Hepatocyte growth factor activator inhibitor type 2 (HAI-2) modulates hepcidin expression by inhibiting the cell surface protease matriptase-2. *Biochem. J.* *450*, 583–593.
- McCoy, A.J., Grosse-Kunstleve, R.W., Adams, P.D., Winn, M.D., Storoni, L.C., and Read, R.J. (2007). Phaser crystallographic software. *J. Appl. Crystallogr.* *40*, 658–674.
- Meynard, D., Vaja, V., Sun, C.C., Corradini, E., Chen, S., López-Otín, C., Grgurevic, L., Hong, C.C., Stirnberg, M., Gütschow, M., et al. (2011). Regulation of TMPRSS6 by BMP6 and iron in human cells and mice. *Blood* *118*, 747–756.
- Nai, A., Pagani, A., Mandelli, G., Lidonnici, M.R., Silvestri, L., Ferrari, G., and Camaschella, C. (2012). Deletion of TMPRSS6 attenuates the phenotype in a mouse model of  $\beta$ -thalassemia. *Blood* *119*, 5021–5029.
- Nai, A., Pellegrino, R.M., Rausa, M., Pagani, A., Boero, M., Silvestri, L., Saglio, G., Roetto, A., and Camaschella, C. (2014). The erythroid function of transferrin receptor 2 revealed by Tmprss6 inactivation in different models of transferrin receptor 2 knockout mice. *Haematologica* *99*, 1016–1021.
- Nemeth, E., Tuttle, M.S., Powelson, J., Vaughn, M.B., Donovan, A., Ward, D.M., Ganz, T., and Kaplan, J. (2004). Hcpicidin regulates cellular iron efflux by binding to ferroportin and inducing its internalization. *Science* *306*, 2090–2093.
- Qvit, N., Rubin, S.J.S., Urban, T.J., Mochly-Rosen, D., and Gross, E.R. (2017). Peptidomimetic therapeutics: scientific approaches and opportunities. *Drug Discov. Today* *22*, 454–462.
- Ramsay, A.J., Reid, J.C., Velasco, G., Quigley, J.P., and Hooper, J.D. (2008). The type II transmembrane serine protease matriptase-2—identification, structural features, enzymology, expression pattern and potential roles. *Front. Biosci.* *13*, 569–579.
- Rausa, M., Ghitti, M., Pagani, A., Nai, A., Campanella, A., Musco, G., Camaschella, C., and Silvestri, L. (2015). Identification of TMPRSS6 cleavage sites of hemojuvelin. *J. Cell. Mol. Med.* *19*, 879–888.
- Rawlings, N.D., Barrett, A.J., Thomas, P.D., Huang, X., Bateman, A., and Finn, R.D. (2018). The MEROPS database of proteolytic enzymes, their substrates and inhibitors in 2017 and a comparison with peptidases in the PANTHER database. *Nucleic Acids Res.* *46*, D624–D632.
- Roydeva, P., Beckmann, A.-M., Stirnberg, M., Cesar, J., Kikelj, D., Ilaš, J., and Gütschow, M. (2016). 3,1-Benzothiazines, 1,4-benzodioxines and 1,4-benzoxazines as inhibitors of matriptase-2: outcome of a focused screening approach. *Pharmaceuticals* *9*, 2.
- Schmidt, P.J., Toudjarska, I., Sendamarai, A.K., Racie, T., Milstein, S., Bettencourt, B.R., Hettlinger, J., Bumcrot, D., and Fleming, M.D. (2013). An RNAi therapeutic targeting Tmprss6 decreases iron overload in Hfe<sup>-/-</sup> mice and ameliorates anemia and iron overload in murine  $\beta$ -thalassemia intermedia. *Blood* *121*, 1200–1208.
- Silvestri, L., Pagani, A., Nai, A., De Domenico, I., Kaplan, J., and Camaschella, C. (2008a). The serine protease matriptase-2 (TMPRSS6) inhibits hepcidin activation by cleaving membrane hemojuvelin. *Cell* *8*, 502–511.

- Silvestri, L., Pagani, A., and Camaschella, C. (2008b). Furin-mediated release of soluble hepcidin: a new link between hypoxia and iron homeostasis. *Blood* 111, 924–931.
- Sisay, M.T., Steinmetzer, T., Stirnberg, M., Maurer, E., Hammami, M., Bajorath, J., and Gütschow, M. (2010). Identification of the first low-molecular-weight inhibitors of matriptase-2. *J. Med. Chem.* 53, 5523–5535.
- St-Georges, C., Désilets, A., Béliveau, F., Ghinet, M., Dion, S.P., Colombo, É., Boudreault, P.-L., Najmanovich, R.J., Leduc, R., and Marsault, É. (2017). Modulating the selectivity of matriptase-2 inhibitors with unnatural amino acids. *Eur. J. Med. Chem.* 129, 110–123.
- Stirnberg, M., Maurer, E., Horstmeyer, A., Kolp, S., Frank, S., Bald, T., Arenz, K., Janzer, A., Prager, K., Wunderlich, P., et al. (2010). Proteolytic processing of the serine protease matriptase-2: identification of the cleavage sites required for its autocatalytic release from the cell surface. *Biochem. J.* 430, 87–95.
- Uhlén, M., Fagerberg, L., Hallström, B.M., Lindskog, C., Oksvold, P., Mardinoglu, A., Sivertsson, Å., Kampf, C., Sjöstedt, E., Asplund, A., et al. (2015). Proteomics. Tissue-based map of the human proteome. *Science* 347, 1260419.
- Valore, E.V., and Ganz, T. (2008). Posttranslational processing of hepcidin in human hepatocytes is mediated by the prohormone convertase furin. *Blood Cells Mol. Dis.* 40, 132–138.
- Vonrhein, C., Flensburg, C., Keller, P., Sharff, A., Smart, O., Paciorek, W., Womack, T., and Bricogne, G. (2011). Data processing and analysis with the *autoPROC* toolbox. *Acta Crystallogr. D Biol. Crystallogr.* 67, 293–302.
- Wahedi, M., Wortham, A.M., Kleven, M.D., Zhao, N., Jue, S., Enns, C.A., and Zhang, A.-S. (2017). Matriptase-2 suppresses hepcidin expression by cleaving multiple components of the hepcidin induction pathway. *J. Biol. Chem.* 292, 18354–18371.
- Wang, C.-Y., Meynard, D., and Lin, H.Y. (2014). The role of TMPRSS6/matriptase-2 in iron regulation and anemia. *Front. Pharmacol.* 5, 114.

## STAR★METHODS

### KEY RESOURCES TABLE

REAGENT or RESOURCE	SOURCE	IDENTIFIER
<b>Antibodies</b>		
Mouse Anti-V5 Monoclonal Antibody	Thermo Fisher Scientific	Cat# R960-25; RRID: AB_2556564
Mouse Anti-V5 Monoclonal Antibody, HRP Conjugated	Thermo Fisher Scientific	Cat# R961-25; RRID: AB_2556565
Rabbit Anti-GAPDH Monoclonal Antibody (14C10), HRP Conjugated	Cell Signaling Technology	Cat# 3683; RRID: AB_1642205
Goat Anti-Hemojuvelin Polyclonal Antibody	R & D Systems	Cat# AF3720; RRID: AB_2264104
Rabbit Anti-Goat IgG (H+L) Secondary Antibody, HRP	Thermo Fisher Scientific	Cat# A16136; RRID: AB_2534807
Horse Anti-Mouse IgG, HRP Conjugated	Cell Signaling Technology	Cat# 7076; RRID: AB_330924
Mouse anti-GAPDH monoclonal Antibody	Sigma-Aldrich	Cat# G8795; RRID: AB_1078991
Rabbit anti-Matriptase2 Antibody	Abcam	Cat# ab28287; RRID: AB_2203535
Goat Anti-Mouse 680LT	LICOR	Cat# 926-68020; RRID: AB_10706161
Goat Anti-Rabbit 800 CW	LICOR	Cat# 926-32211; RRID: AB_621843
<b>Bacterial and Virus Strains</b>		
Bacmam/TMPRSS6-WT isoform 2	This paper	N/A
Bacmam/TMPRSS6-S762A isoform 2	This paper	N/A
<b>Biological Samples</b>		
Human Plateable Hepatocytes, Induction Qualified	ThermoFisher Scientific	Cat# HMCPIP, Lot# Hu1797, Hu1836, Hu1880, Hu8148, Hu8279
<b>Chemicals, Peptides, and Recombinant Proteins</b>		
Boc-Gln-Ala-Arg-AMC	R & D Systems	Cat# ES014
Boc-Ile-Glu-Gly-Arg-AMC acetate salt	Bachem	Cat# 4004961
Boc-Arg-Val-Arg-Arg-AMC acetate salt	Bachem	Cat# 4018735
4-Methylumbelliferyl 4-guanidinobenzoate Hydrochloride (MUGB-HCl)	Santa Cruz Biotechnology	Cat# sc-210120
Compound-2	( <a href="#">St-Georges et al., 2017</a> )	N/A
Compound-8	( <a href="#">St-Georges et al., 2017</a> )	N/A
Compound-29	( <a href="#">St-Georges et al., 2017</a> )	N/A
Compound-A	This paper	N/A
Compound-B	This paper	N/A
William's E Medium, no phenol red	ThermoFisher Scientific	Cat# A1217601
Primary Hepatocyte Thawing and Plating Supplements	ThermoFisher Scientific	Cat# CM3000
Primary Hepatocyte Maintenance Supplements	ThermoFisher Scientific	Cat# CM4000
Cryopreserved Hepatocyte Recovery Medium (CHRM)	ThermoFisher Scientific	Cat# CM7000
High glucose Dulbecco's Modified Eagle's Medium (DMEM)	WISENT Bioproducts	Cat# 319-005-CL
Eagle's Minimum Essential Medium (EMEM)	WISENT Bioproducts	Cat# 320-005-CL
HCell-100	WISENT Bioproducts	Cat# 001-035-CL
Fetal bovine serum (FBS)	WISENT Bioproducts	Cat# 080-150
Penicillin-Streptomycin L-Glutamine	WISENT Bioproducts	Cat# 450-202-EL
Lipofectamine 3000 Transfection Reagent	ThermoFisher Scientific	Cat# L3000015
Complete Protease Inhibitor Cocktail	Sigma-Aldrich	Cat# 11836145001
Recombinant Human BMP-6 Protein	R & D Systems	Cat# 507-BP-020
Clarity Western ECL Substrate	Bio-Rad	Cat# 1705060
Basal Medium Eagle (BME)	Thermo Fisher Scientific	Cat#21010046
Insulin-Transferrin-Selenium (ITS-G) 100X	Thermo Fisher Scientific	Cat# 41400045

(Continued on next page)

**Continued**

REAGENT or RESOURCE	SOURCE	IDENTIFIER
Recombinant Human BMP6 (Carrier-free)	TONBO Biosciences	Cat# 21-7004-U100
Recombinant Human TMPRSS6	GlaxoSmithKline	
Recombinant Human Coagulation Factor Xa Protein, CF	R & D Systems	Cat# 1063-SE-010
Thrombin from Human Plasma, High Activity	Millipore Sigma	Cat# 605195
Recombinant Human Furin Protein, CF	R & D Systems	Cat# 1503-SE-010
Restore™ PLUS Western Blot Stripping Buffer	Thermo Fisher Scientific	Cat# 46430
TMB One Component Substrate	Bethyl	Cat# E102
3,3',5,5'-Tetramethylbenzidine Liquid Substrate	Sigma	Cat# T4319
Transcriptor First Strand cDNA Synthesis Kit	Roche	Cat# 04897030001
RNaseOUT Recombinant Ribonuclease Inhibitor	Thermo Fisher Scientific	Cat# 10777019
iTaq Universal SYBR® Green Supermix	Bio-Rad	Cat# 1725120
TRIzol Reagent	Thermo Fisher Scientific	Cat# 15596018
RIPA Lysis Buffer	Thermo Fisher Scientific	Cat# 89900
Odyssey® One-Color Protein Molecular Weight Marker	LICOR	Cat# 928-40000
Odyssey® Blocking Buffer in TBS	LICOR	Cat# 927-50000
<b>Critical Commercial Assays</b>		
Hepcidin-25 (Human) EIA kit	Peninsula Laboratories	Cat# S-1337
Cells-to-CT 1-Step TaqMan Kit	Thermo Fisher Scientific	Cat# A25602
CellTiter-Glo Luminescent Cell Viability Assay	Promega	Cat# G7572
Cytotoxicity Detection Kit <sup>PLUS</sup> (LDH)	Roche	Cat# 04744926001
Pierce Cell Surface Protein Isolation Kit	Thermo Fisher Scientific	Cat# 89881
Pierce BCA Protein Assay Kit	Thermo Fisher Scientific	Cat# 23227
<b>Deposited Data</b>		
Matriptase/Compound-8 structure	This study	PDB: 6N4T
Crystal Structure of MT-SP1 bound to Benzamidine Phosphonate Inhibitor	( <a href="#">Brown et al., 2011</a> )	PDB: 3NCL
Crystal Structure of Matriptase in complex with Inhibitor	( <a href="#">Goswami et al., 2013</a> )	PDB: 4JYT
<b>Experimental Models: Cell Lines</b>		
HEK293	ATCC	Cat# CRL-1573; RRID: CVCL_0045
HepG2	ATCC	Cat# HB-8065; RRID: CVCL_002
<b>Oligonucleotides</b>		
HAMP TaqMan Assay (Human)	Thermo Fisher Scientific	Cat# 4331182/Hs00221783_m1
B2M TaqMan Assay (Human)	Thermo Fisher Scientific	Cat# 4331182/Hs99999907_m1
PPIA TaqMan Assay (Human)	Thermo Fisher Scientific	Cat# 4331182/Hs99999904_m1
Additional oligonucleotides are described in <a href="#">Table S5</a>		
<b>Recombinant DNA</b>		
pcDNA6/V5	( <a href="#">Béliveau et al., 2011</a> )	N/A
pcDNA6/TMPRSS6-WT-V5 isoform 1/V5	( <a href="#">Béliveau et al., 2011</a> )	N/A
pcDNA6/TMPRSS6-S762A-V5 isoform 1/V5	( <a href="#">Béliveau et al., 2011</a> )	N/A
pcDNA6/TMPRSS6-WT-V5 isoform 2/V5	( <a href="#">Dion et al., 2018a</a> )	N/A
pcDNA6/TMPRSS6-S762A-V5 isoform 2/V5	( <a href="#">Dion et al., 2018a</a> )	N/A
pCMV6-Entry/HJV variant a	Origene	Cat# RC217954
pET28a/ST14 (aa 615-855)	This study	N/A
<b>Software and Algorithms</b>		
GraphPad Prism 7	GraphPad	Version 7.04 for Windows
GraphPad Prism 8	GraphPad	Version 8.0.2 for Windows

(Continued on next page)

**Continued**

REAGENT or RESOURCE	SOURCE	IDENTIFIER
Molecular Operating Environment (MOE)	Chemical Computing Group	Version 2013.08
Bio-1D	Vilber Lourmat	Version 15.05
IDBS ActivityBase software	IDBS	N/A
Other		
Amicon Ultra-0.5 Centrifugal Filter Unit (10,000 NMWL)	Millipore Sigma	Cat# UFC501096
RNeasy Mini Kit	Qiagen	Cat# 74106

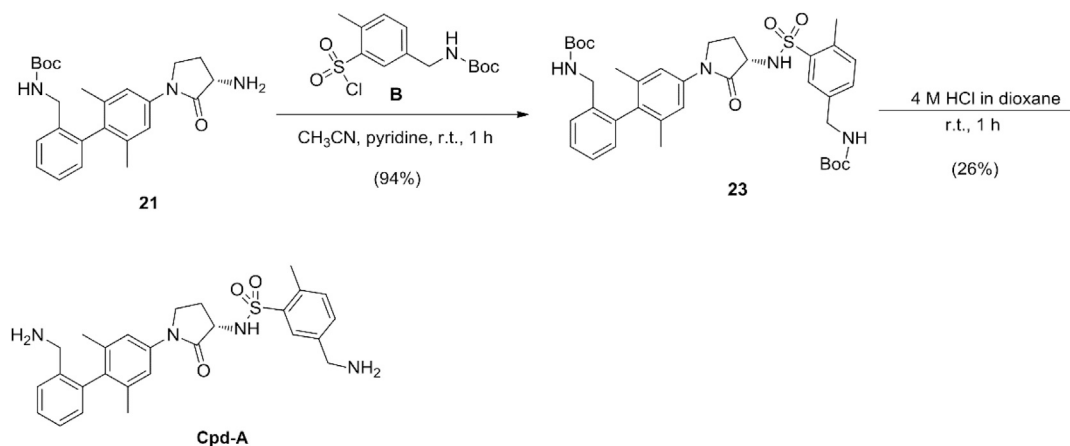
**LEAD CONTACT AND MATERIALS AVAILABILITY**

Please contact Richard Leduc, Université de Sherbrooke, 3001, 12<sup>e</sup> Avenue Nord, Sherbrooke, Québec, Canada J1H 5N4. e-mail: [Richard.Leduc@USherbrooke.ca](mailto:Richard.Leduc@USherbrooke.ca), phone: +1 (819) 821-8000 ext. 75413, Fax: +1 (819) 564-5400 for reagents and resources generated in this study.

**EXPERIMENTAL MODEL AND SUBJECT DETAILS**

**Chemical Synthesis of Compounds**

**Synthesis of Cpd-A**

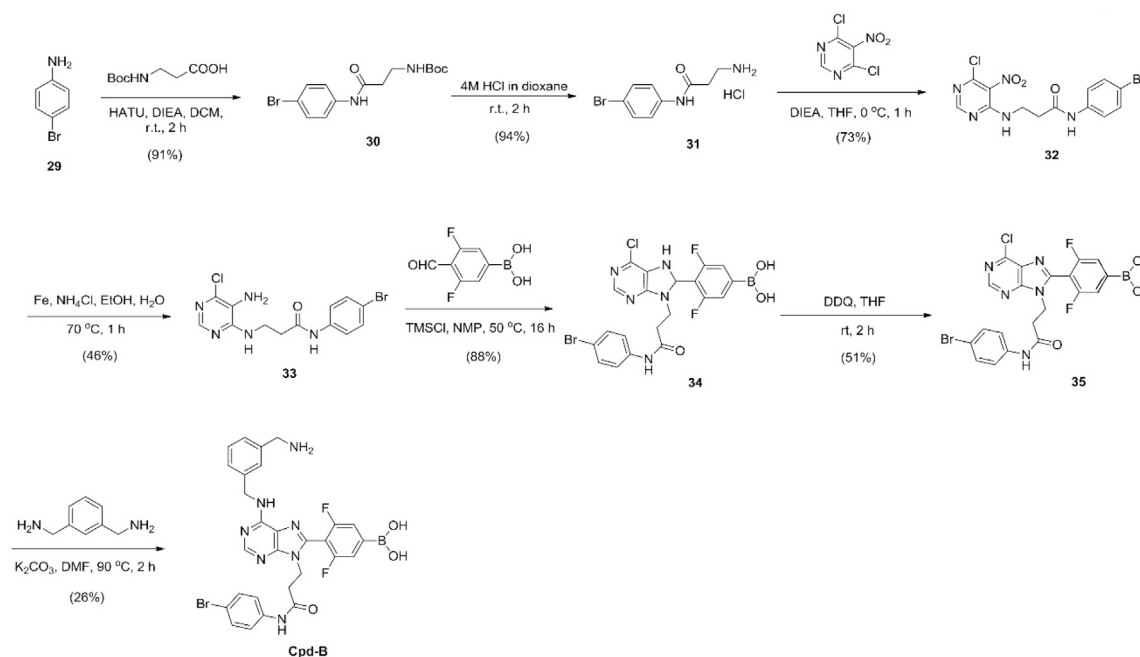


**Synthesis of (S)-tert-butyl ((4'-(3-((tert-butoxycarbonyl)amino)methyl)-2-methylphenyl)sulfonamido)-2-oxopyrrolidin-1-yl)-2',6'-dimethyl-[1,1'-biphenyl]-2-yl)methyl)carbamate (23).** Tert-butyl 3-(chlorosulfonyl)-4-methylbenzylcarbamate (**B**) (330 mg, 1.03 mmol) was dissolved in acetonitrile (21 mL), then pyridine (2.2 mL) was added followed by (S)-tert-butyl ((4'-(3-amino-2-oxopyrrolidin-1-yl)-2',6'-dimethyl-[1,1'-biphenyl]-2-yl)methyl)carbamate (**21**) (384 mg, 0.94 mmol). After stirring at room temperature for 1 h, the mixture was poured in water (300 mL), extracted with ethyl acetate (3 x 200 mL), dried over Na<sub>2</sub>SO<sub>4</sub>, filtered, and concentrated in vacuum. The residue (700 mg, yellow solid) was purified by thin layer chromatography, developed with petroleum:ethyl acetate=3:2. This afforded (S)-tert-butyl ((4'-(3-((tert-butoxycarbonyl)amino)methyl)-2-methylphenyl)sulfonamido)-2-oxopyrrolidin-1-yl)-2',6'-dimethyl-[1,1'-biphenyl]-2-yl)methyl)carbamate (**23**) (610 mg, 94%, purity: 97%) as a white solid. <sup>1</sup>HNMR (400 MHz, CDCl<sub>3</sub>): δ 7.98 (s, 1H), 7.47-7.43 (m, 2H), 7.36-7.30 (m, 5H), 7.00-6.98 (m, 1H), 4.98 (br, 1H), 4.57 (br, 1H), 4.36 (br, 2H), 3.93-3.90 (m, 2H), 3.85-3.77 (m, 3H), 2.77 (s, 3H), 2.71 2.64 (m, 1H), 2.18-2.10 (m, 1H), 1.96 (s, 6H), 1.49 (s, 9H), 1.42 (s, 9H). LCMS (ESI): m/z 715 [M+H]<sup>+</sup>.

**Synthesis of (S)-5-(aminomethyl)-N-(1-(2'-(aminomethyl)-2,6-dimethyl-[1,1'-biphenyl]-4-yl)-2-oxopyrrolidin-3-yl)-2-methylbenzenesulfonamide (Cpd-A).** (S)-Tert-butyl ((4'-(3-((tert-butoxycarbonyl)amino)methyl)-2-methylphenyl)sulfonamido)-2-oxopyrrolidin-1-yl)-2',6'-dimethyl-[1,1'-biphenyl]-2-yl)methyl)carbamate (**23**) (600 mg, 0.87 mmol) was dissolved in HCl/dioxane (4 M, 10 mL) and the mixture was stirred for 1 h at room temperature after which the solvent was removed in vacuum, and the residue (800 mg, white solid) was dissolved in MeOH (5 mL). The mixture was purified with the following conditions: Column, XBridge Prep C18 OBD Column 19x150 mm, 5 μm; Mobile Phase A: water (0.05% TFA), Mobile Phase B: ACN; Flow Rate: 25 mL/min; Gradient: 5% B to 30% B in

10 min; 254 nm; Rt: 8.25 min. This afforded (S)-5-(aminomethyl)-N-(1-(2'-(aminomethyl)-2,6-dimethyl-[1,1'-biphenyl]-4-yl)-2-oxopyrrolidin-3-yl)-2-methylbenzenesulfonamide (**Cpd-A**, bis-TFA salt) (160 mg, 26% yield, purity: 99%, %ee: 100) as a white solid. <sup>1</sup>HNMR (400 MHz, CD<sub>3</sub>OD): δ 8.23 (d, *J* = 2.0 Hz, 1H), 7.62–7.50 (m, 5H), 7.41–7.40 (m, 2H), 7.15–7.12 (m, 1H), 4.26–4.19 (m, 3H), 3.84–3.80 (m, 2H), 3.76 (s, 2H), 2.78 (s, 3H), 2.67–2.47 (m, 1H), 2.11–2.00 (m, 1H), 1.97 (s, 6 H). LCMS (ESI): *m/z* 493 [M+H]<sup>+</sup>. <sup>19</sup>FNMR (300 MHz, CD<sub>3</sub>OD): δ: -76.93, -76.90.

### Synthesis of Cpd-B



**Synthesis of tert-butyl 3-((4-bromophenyl)amino)-3-oxopropyl)carbamate (30).** To a solution of 4-bromoaniline (12 g, 70.6 mmol) in dichloromethane (120 mL) at room temperature was added 3-((tert-butoxycarbonyl) amino) propanoic acid (16 g, 84.7 mmol), HATU (40 g, 105 mmol), and diisopropylethylamine (45 g, 349 mmol). After 2 h water (100 mL) was added, and the aqueous phase was extracted with dichloromethane (2 × 100 mL). The combined organic extracts were dried over anhydrous sodium sulfate, filtered, and concentrated. Purification by silica gel chromatography (ethyl acetate: petroleum ether= 1:1) afforded tert-butyl 3-((4-bromophenyl) amino)-3-oxopropyl)carbamate (**30**) (22 g, 91% yield, purity: 100%) as a yellow solid. <sup>1</sup>HNMR (300 MHz, DMSO-*d*<sub>6</sub>): δ 10.06 (s, 1H), 7.59–7.55 (m, 2H), 7.49–7.45 (m, 2H), 6.88 (t, *J* = 5.6 Hz, 1H), 3.24–3.18 (m, 2H), 2.47–2.44 (m, 2H), 1.38 (s, 9H). LCMS (ESI): *m/z* 343 [M+H]<sup>+</sup>.

**Synthesis of 3-amino-N-(4-bromophenyl)propanamide (31).** 4M HCl in 1,4-dioxane (120 mL) was added to tert-butyl 3-((4-bromophenyl)amino)-3-oxopropyl)carbamate (**30**) (12 g, 35.1 mmol) at room temperature. After 2 h, the solvent was removed under reduced pressure to afford 3-amino-N-(4-bromophenyl)propanamide, HCl salt (**31**) (9.2 g, 94% yield, purity: 97%). <sup>1</sup>HNMR (400 MHz, DMSO-*d*<sub>6</sub>): δ 10.59 (br, 1H), 8.07 (br, 3H), 7.64–7.60 (m, 2H), 7.51–7.47 (m, 2H), 3.09–3.04 (m, 2H), 2.81–2.75 (m, 2H). LCMS (ESI): *m/z* 242 [M+H]<sup>+</sup>.

**Synthesis of N-(4-bromophenyl)-3-((6-chloro-5-nitropyrimidin-4-yl)amino)propanamide (32).** To a solution of 3-amino-N-(4-bromophenyl)propanamide, HCl salt (**31**) (5.5 g, 19.8 mmol) and diisopropylethylamine (12.8 g, 99.2 mmol) in THF (150 mL) at 0°C was added a solution of 4,6-dichloro-5-nitropyrimidine (4.6 g, 23.8 mmol) in THF (100 mL) dropwise. After 1 h at 0°C the solvent was removed under reduced pressure. The residue was then diluted with water (100 mL), extracted with ethyl acetate (100 mL × 3), and the combined organic extracts were dried over anhydrous sodium sulfate, filtered, and concentrated. Purification by silica gel chromatography (ethyl acetate: petroleum ether= 1:1) afforded N-(4-bromophenyl)-3-((6-chloro-5-nitropyrimidin-4-yl)amino)propanamide (**32**) (5.8 g, 73% yield, purity: 96%) as a yellow solid. <sup>1</sup>HNMR (400 MHz, DMSO-*d*<sub>6</sub>): δ 10.23 (s, 1H), 9.73 (t, *J* = 5.9 Hz, 1H), 8.12 (s, 1H), 7.58–7.56 (m, 2H), 7.49–7.47 (m, 2H), 3.90–3.85 (m, 2H), 2.72–2.65 (m, 2H). LCMS (ESI): *m/z* 399 [M+H]<sup>+</sup>.

**Synthesis of 3-((5-amino-6-chloropyrimidin-4-yl)amino)-N-(4-bromophenyl)propanamide (33).** To a solution of N-(4-bromophenyl)-3-((6-chloro-5-nitropyrimidin-4-yl)amino)propanamide (**32**) (1.5 g, 3.76 mmol) in ethanol (60 mL) and water (15 mL) was added iron(0) (2.1 g, 37.5 mmol) and NH<sub>4</sub>Cl (994 mg, 18.6 mmol) and the reaction heated to 70°C. After 1 h the mixture was allowed to cool to room temperature, filtered, and concentrated. The residue was diluted with water (100 mL), extracted with ethyl acetate (100 mL × 3), and

the combined organic extracts were dried over anhydrous sodium sulfate, filtered, and concentrated. Purification by silica gel chromatography (methanol: dichloromethane= 1:10) afforded 3-((5-amino-6-chloropyrimidin-4-yl)amino)-N-(4-bromophenyl)propanamide (**33**) (640 mg, 46% yield, purity: 98%) as a yellow solid. <sup>1</sup>HNMR (400 MHz, DMSO-*d*<sub>6</sub>): δ 10.08 (s, 1H), 7.76 (s, 1H), 7.60-7.56 (m, 2H), 7.49-7.45 (m, 2H), 6.99 (t, *J* = 5.5 Hz, 1H), 5.05 (s, 2H), 3.69-3.65 (m, 2H), 2.65 (t, *J* = 6.6 Hz, 2H). LCMS (ESI): *m/z* 370 [M+H]<sup>+</sup>. **Synthesis of (4-(9-(3-((4-bromophenyl)amino)-3-oxopropyl)-6-chloro-8,9-dihydro-7H-purin-8-yl)-3,5-difluorophenyl)boronic acid (34).** To a solution of 3-((5-amino-6-chloropyrimidin-4-yl)amino)-N-(4-bromophenyl)propanamide (**33**) (600 mg, 1.63 mmol) in NMP (12 mL) was added 3,5-difluoro-4-formylphenylboronic acid (361 mg, 1.94 mmol) and TMSCI (875 mg, 8.1 mmol) and the reaction was heated to 50°C. After 16 h, the mixture was diluted with water (100 mL), extracted with ethyl acetate (100 mL × 3), and the combined organic extracts were washed with saturated brine (150 mL × 3), dried over anhydrous sodium sulfate, filtered and concentrated to afford (4-(9-(3-((4-bromophenyl)amino)-3-oxopropyl)-6-chloro-8,9-dihydro-7H-purin-8-yl)-3,5-difluorophenyl)boronic acid (**34**) as a yellow solid (760 mg, 88% yield, purity: 71%). <sup>1</sup>HNMR (300 MHz, DMSO-*d*<sub>6</sub>): δ 10.11-10.07 (m, 1H), 8.47 (s, 1H), 7.70 (s, 1H), 7.40-7.33 (m, 4H), 6.75-3.78 (m, 2H), 4.05-3.98 (m, 1H), 3.71-3.63 (m, 1H), 3.26-3.17 (m, 1H), 2.74-2.64 (m, 1H), 2.55-2.52 (m, 1H). LCMS (ESI): *m/z* 538 [M+H]<sup>+</sup>.

**Synthesis of (4-(9-(3-((4-bromophenyl)amino)-3-oxopropyl)-6-chloro-9H-purin-8-yl)-3,5-difluorophenyl)boronic acid (35).** To a solution of (4-(9-(3-((4-bromophenyl)amino)-3-oxopropyl)-6-chloro-8,9-dihydro-7H-purin-8-yl)-3,5-difluorophenyl)boronic acid (**34**) (760 mg, 1.4 mmol) in THF (12 mL) was added DDQ (636 mg, 2.8 mmol). After stirring at room temperature for 2 h, the solvent was removed under reduced pressure. The residue was then dissolved in DMF (6 mL) and purified by reversed phase HPLC with the following conditions: Column: C18 silica gel 80 g, 20-35 μm; Mobile Phase A: Water (0.05% TFA), Mobile Phase B: ACN; Flow rate: 50 mL/min; Gradient: 5% B to 55% B in 20 min; 254 nm. This afforded (4-(9-(3-((4-bromophenyl)amino)-3-oxopropyl)-6-chloro-9H-purin-8-yl)-3,5-difluorophenyl)boronic acid (**35**) (380 mg, 51% yield, purity: 100%) as a yellow solid. <sup>1</sup>HNMR (300 MHz, DMSO-*d*<sub>6</sub>): δ 10.06-10.04 (m, 1H), 8.90-8.89 (m, 1H), 7.78 (d, *J* = 8.5 Hz, 1H), 7.60 (dd, *J* = 17.1, 8.7 Hz, 1H), 7.42-7.34 (m, 4H), 4.54-4.46 (m, 2H), 4.10 (s, 2H), 2.96-2.88 (m, 2H). LCMS (ESI): *m/z* 536 [M+H]<sup>+</sup>.

**Synthesis of (4-(6-((3-(aminomethyl)benzyl)amino)-9-(3-((4-bromophenyl)amino)-3-oxopropyl)-9H-purin-8-yl)-3,5-difluorophenyl)boronic acid (Cpd-B).** To a solution of (4-(9-(3-((4-bromophenyl)amino)-3-oxopropyl)-6-chloro-9H-purin-8-yl)-3,5-difluorophenyl)boronic acid (**35**) (280 mg, 0.52 mmol) in DMF (9 mL) was added 1,3-phenylenedimethanamine (354 mg, 2.6 mmol) and K<sub>2</sub>CO<sub>3</sub> (359 mg, 2.6 mmol) and the mixture was heated to 90°C. After 2 h the mixture was allowed to cool to room temperature, filtered and submitted to HPLC purification with the following conditions: Column: XBridge Prep C18 OBD Column 19 × 150 mm; 5 μm; Mobile Phase A: Water (0.05% TFA), Mobile Phase B: ACN; Flow rate: 25 mL/min; Gradient: 17% B to 37% B in 8 min; 254 nm; Rt: 6.55 min. This afforded (4-(6-((3-(aminomethyl)benzyl)amino)-9-(3-((4-bromophenyl)amino)-3-oxopropyl)-9H-purin-8-yl)-3,5-difluorophenyl)boronic acid (**Cpd-B**, TFA salt) (102 mg, 26% yield, purity: 100%) as a white solid. <sup>1</sup>HNMR (300 MHz, DMSO-*d*<sub>6</sub>): δ 8.37 (s, 1H), 7.50-7.43 (m, 3H), 7.39-7.31 (m, 7H), 4.86 (s, 2H), 4.53 (t, *J* = 4.0 Hz, 2H), 4.09 (s, 2H), 2.87 (t, *J* = 4.2 Hz, 2H). LCMS (ESI): *m/z* 636 [M+H]<sup>+</sup>. <sup>19</sup>FNMR (300 MHz, DMSO-*d*<sub>6</sub>): δ: -113.30, -77.23.

## Cell Culture

HEK293 cells were grown in High glucose Dulbecco's Modified Eagle's Medium (DMEM), HepG2 were grown in Eagle's Minimum Essential Medium (EMEM), both media were supplemented with 10% fetal bovine serum (FBS), 2 mM L-glutamine, 1 mM sodium pyruvate, 100 IU/mL penicillin and 100 μg/mL streptomycin.

HepG2 cells for qPCR analysis were grown in Basal Eagle's Medium (BME) supplemented with 10% FBS, 2 mM L-glutamine, 1 mM sodium pyruvate and 1X ITS. After incubation overnight at 37°C for cell attachment, cell medium was replaced with the same media without serum.

Cryopreserved human primary hepatocytes are from different donors: Hu1797 (Caucasian male, 77-year-old), Hu1836 (Caucasian female, 66-year-old), Hu8148 (Caucasian female, 55-year-old) and Hu8279 (Caucasian female, 53-year-old). Cells were thaw in a 37°C water bath for 2 min, transferred in pre-warmed Cryopreserved Hepatocyte Recovery Medium (CHRM) and centrifuged at 100 *g* for 10 min at room temperature. Pelleted cells were resuspended in Plating Medium (William's E Medium without phenol red supplemented with Primary Hepatocyte Thawing and Plating Supplements). After overnight incubation at 37°C for cell attachment, cell medium was replaced with Maintenance Medium (William's E Medium without phenol red supplemented with Primary Hepatocyte Maintenance Supplements).

The human biological samples were sourced ethically, and their research use was in accord with the terms of the informed consents under an IRB/EC approved protocol.

## METHOD DETAILS

### Screening of Inhibitory Potency in Cells

HEK293 cells were transfected with mock (pcDNA6/V5), TMPRSS6 WT (pcDNA6/TMPRSS6-WT-V5 isoform 1/V5) (UniProt Q8IU80-4) or TMPRSS6 S762A (pcDNA6/TMPRSS6-S762A-V5 isoform 1/V5) cDNA using Lipofectamine 3000 in 6-well plates. After 24h transfection, cell media were replaced with HCell-100 media containing vehicle (DMSO 0.1%) or 100 nM compound (Table S1) for 24h. Cell media was collected, and cells were lysed in lysis buffer (1% Triton, 50 mM Tris, 150 mM NaCl, 5 mM EDTA) supplemented with Protease Inhibitor Cocktail.

For proteolytic activity measurements, release of fluorescence (excitation, 360 nm; emission 460 nm) with 200  $\mu$ M Boc-QAR-AMC was measured for 1 h at room temperature in an FLx800 TBE microplate reader (Bio-Tek Instruments) in collected cell media. Proteolytic activities (mF.U/min) were normalized to protein quantity in cell lysate (mF.U/min per  $\mu$ g of protein) and reported on vehicle-treated TMPRSS6-transfected cells activity and expressed as residual activity (%).

For TMPRSS6 immunodetection in cell media, 1 mL of media was concentrated using centrifugal filters (10,000 NMWL, 21,100 g, 15 min, 4°C). Concentrated samples were loaded on 12% SDS-polyacrylamide gels under denaturing conditions. As loading and TMPRSS6 expression controls, 30  $\mu$ g of cell lysates were loaded on 12% SDS-polyacrylamide gels. Migrated proteins were electro-transferred onto PVDF membranes. Nonspecific protein binding was blocked using a solution of 10% skimmed milk in TBS 0.1% Tween-20. Primary antibodies, anti-V5-HRP for concentrated cell media and cell lysate; and anti-GAPDH-HRP for cell lysate, were diluted in 5% skimmed milk in TBS 0.1% Tween-20 and incubated overnight at 4°C. After three sequential washing steps (5 min each) with TBS 0.1% Tween-20, Clarity Western ECL substrate (Bio-Rad) was put on membranes and blot images were acquired using a Fusion Pulse system (Vilber Lourmat).

### Compounds IC<sub>50</sub> on TMRSS6 Activity In Cellulo

HEK293 cells were reverse transfected with mock (pcDNA6/V5) or previously described TMPRSS6 WT (pcDNA6/TMPRSS6-WT-V5 isoform 2/V5) (UniProt Q8IU80-2) cDNA (Dion et al., 2018a) using Lipofectamine 3000 in 96-well plates. After 24h transfection, cell media were washed twice with PBS and HCell-100 media containing vehicle (DMSO 0.1%) or compound was added. For all compounds, 10 tree-fold serial dilutions were tested. The highest doses were 900 nM for Cpd-2 and Cpd-29, 300 nM for Cpd-8 and 30  $\mu$ M for Cpd-A and Cpd-B. After 24h, cell media was collected and proteolytic activities were measured in cell media using Boc-QAR-AMC (mF.U/min). IC<sub>50</sub> values were derived by a sigmoidal dose-response (variable slope) curve using GraphPad Prism 8 software from a log([Compound]) versus cell media proteolytic activity plot. GraphPad was used to identify and eliminate outliers (Q=1) and to assess the goodness of the fits. Only curves presenting a R squared  $\geq$  0.8 were used for the mean IC50 calculation. All assays were performed at least three times and data are presented as mean  $\pm$  standard deviation (SD).

### In Vitro IC<sub>50</sub> Determination

Recombinant human TMPRSS6, matriptase and hepsin were expressed and purified as described previously (Béliveau et al., 2009). Recombinant human factor Xa, and furin (R & D Systems) as well as human thrombin from plasma (Millipore Sigma) were obtained from commercial sources. Enzymatic assays were all performed at room temperature in an assay buffer containing 50 mM HEPES pH 7.4, 1 mM  $\beta$ -mercaptoethanol, 1 mM CaCl<sub>2</sub> and 500  $\mu$ g/ml BSA for furin and 50 mM HEPES pH 7.4, 150 mM NaCl and 500  $\mu$ g/ml BSA for all other proteases. All assays were performed using a fluorogenic substrate (Boc-RVRR-AMC for furin, Boc-IEGR-AMC for factor Xa and Boc-QAR-AMC for other proteases) at a concentration equivalent to the Michaelis constant K<sub>M</sub>. To determine IC<sub>50</sub>, 1 nM (TMPRSS6, matriptase, hepsin, thrombin) or 2 nM (factor Xa, furin) was added to a reaction buffer containing serial-diluted inhibitor and the fluorogenic substrate. Proteolytic activity was then monitored by measuring the release of fluorescence (excitation, 360 nm; emission, 441 nm) in a FLX800 TBE microplate reader (BioTek Instruments) for 1 h. All velocities were retrieved, and data were fitted by non-linear regression analysis to an inhibitory dose-response curve according to the variable slope model (four-parameter, 4PL). All assays were performed at least three times and data are presented as mean  $\pm$  standard deviation (SD). Nonlinear regression and statistical analysis were performed using GraphPad Prism version 7.04 for Windows (GraphPad Software, La Jolla California USA, [www.graphpad.com](http://www.graphpad.com)).

### Compound Toxicity In Cellulo

HEK293, HepG2 and human primary hepatocytes (Hu1880) were seeded in 96 well-plates. After 24h plating, cells were washed with PBS and media containing vehicle or compound was added to cells. For HEK293 cells, Cpd-2, -8 and -29 were tested at 10  $\mu$ M and Cpd-A and -B were tested at 30  $\mu$ M. HepG2 cells and human primary hepatocytes were tested with Cpd-8, -A and -B at 10  $\mu$ M. After 24h exposure to compounds, lactate dehydrogenase (LDH) release was measured at 492 nm using Roche's Cytotoxicity Detection Kit<sup>PLUS</sup> (LDH) as recommended by the manufacturer. For each cell lines, assays were performed in triplicate, three times. Results are background corrected and presented as the mean Cytotoxicity (%) compared to lysed cells  $\pm$  standard deviation (SD).

### Compound Effect on Cell Surface Expression in HEK293 Cells

HEK293 cells were seeded on collagen-coated 24 well plates. 24h post-plating, cells were washed with PBS and transfected with mock (pcDNA6/V5) or TMPRSS6 WT (pcDNA6/TMPRSS6-WT-V5 isoform 2/V5) (UniProt Q8IU80-2) cDNA using Lipofectamine 3000. After 24h transfection, cells were washed twice with PBS and incubated with HCell media containing compound or vehicle. Concentrations tested were 10  $\mu$ M for Cpd-2, -8 and -29 and 30  $\mu$ M for Cpd-A and -B. After 24h treatment, cell media were removed, cells fixed in 3.7% formaldehyde, diluted in PBS, for 5 min at room temperature (RT). Cells were washed with PBS prior to blocking in PBS-10% skimmed milk for 1h at RT. Blocking solution was removed and cells incubated with 500  $\mu$ L of anti-V5 primary antibody (1:500) diluted in PBS-5% skimmed milk for 1h at RT. The primary antibody containing solution was removed and cells washed twice with PBS prior incubation with horse anti-mouse HRP conjugated antibody (1:2000) diluted in PBS-5% skimmed milk for 1h at RT. Cells were washed twice with PBS and incubated with 3,3',5,5'-tetramethylbenzidine (TMB) for 5 min prior to stopping the reaction with 500  $\mu$ L of HCl 2N. Absorbance was measured at 450 nm. Results are background corrected and presented as cell surface expression fold over vehicle treated cells  $\pm$  standard deviation (SD).

### Compound Effect on Cell Surface Expression in HepG2 Cells

HepG2 cells were transfected with 5  $\mu$ g of TMPRSS6 WT (pcDNA6/TMPRSS6-WT-V5 isoform 2/V5) (UniProt Q8IU80-2) and same quantity of mock (pcDNA6/V5) or pCMV6-Entry/HJV variant a (UniProt Q6ZVN8-1) cDNA using Lipofectamine 3000. After a 24-h transfection, biotinylation of HepG2 surface proteins was performed with Pierce cell-surface protein isolation kit. Equal quantities of proteins from cell lysate were precipitated (biotinylated cell-surface proteins) or not (total proteins) with avidin and the resulting samples were loaded on a 10% SDS-polyacrylamide gels under denaturing conditions. Migrated proteins were electro-transferred onto nitrocellulose membranes. Nonspecific protein binding was blocked using a solution of 5% bovine serum albumin (HJV) or 10% skim milk (V5) in TBS 0.1% Tween-20. Anti-HJV antibodies were diluted in a solution of 2.5% BSA in TBS 0.1% Tween-20, anti-V5 and anti-GAPDH-HRP antibodies were diluted in a solution of 5% skim milk in TBS 0.1% Tween-20. All membranes were incubated 1 h at RT. For anti-HJV and anti-V5 antibodies, after three sequential washing steps (5 min each) with TBS 0.1% Tween-20, membranes were incubated with horseradish peroxidase-conjugated secondary antibodies (Rabbit anti-Goat for anti-HJV or Horse anti-mouse for anti-V5) for 1 h at RT and washed three times (5 min) in TBS 0.1% Tween-20. Clarity Western ECL substrate was used on membranes and blot images were acquired using a Fusion Pulse system. Band intensities were quantified by densitometry analysis using Bio-1D software (Vilber Lourmat), normalized with GAPDH expression and reported on vehicle-treated cells (0.1 % DMSO).

### Matriptase/Cpd-8 Crystal Structure

Crystallization of matriptase (ST14) with Cpd-8 was performed at the Contract Research Organization (CRO), Aurigene Discovery Technologies Limited using previously described methods (Goswami et al., 2013). In brief, matriptase (ST14) (GenBank: AF057145, GenBank: NM\_021978.3) residues 615 to 855 were cloned into pET28a. Over expression was performed by induction of mid-log phase BL21 DE3 *Escherichia coli* cells with 1 mM isopropyl-1-thio- $\beta$ -D-galactopyranoside for 4 hrs at 37°C. Cell pellets were washed with lysis buffer (10 mM Tris pH 8.0, 150 mM NaCl and 2 mM DTT) and treated with 50  $\mu$ g/mL lysozyme for 30 min. The cells lysed by sonication and the cell debris cleared by centrifugation at 12 000 rpm for 20 min at 4°C. The inclusion bodies were washed thoroughly with buffer (10 mM Tris pH 8.0, 150 mM NaCl). Pellets were then solubilized in a buffer containing 10 mM Tris pH 8.0, 150 mM NaCl, 6 M Guanidinium chloride, 100 mM sodium phosphate pH 8 for 4 hrs by stirring at room temperature. Solubilized protein was diluted in a buffer consisting of 50 mM Tris pH 8.0, 100 mM NaCl, 0.5 M Arginine, 0.2 mM GSSH (Oxidized glutathione), 2 mM GSH (Reduced glutathione), 20 mM  $\text{CaCl}_2$ , 1 mM EDTA and 1 M Urea at 4°C for 72 hrs. Protein was dialyzed against 15 volumes of dialysis buffer (25 mM Tris pH 8, 50 mM NaCl and 1 M Urea) at 4°C. The dialyzed protein was subjected to anion-exchange column chromatography (HiTrap Q FF, GE Healthcare) and the bound protein eluted by step gradient using buffer 25 mM Tris pH 8.0, 1 M NaCl using AKTA FPLC (GE Healthcare) system. Refolded protein was eluted between 50-150 mM of NaCl concentration was later passed through superdex-75 column (GE Healthcare) using 50 mM Tris pH 8.0, 500 mM NaCl.

Crystals were grown by Aurigene. Protein was concentrated with benzamidine to 30 mg/mL and crystallization was setup under conditions with reservoir solution (0.1 Tris, pH 8.2-8.7, PEG800 (18% - 22%) and 200 mM  $\text{MgCl}_2$ ) using hanging drop vapor diffusion at room temperature. Crystals grew overnight, were harvested and soaked into a solution with Cpd-8. The crystals were transferred to a cryo-protectant and flash frozen at 100 K. The crystals were sent to the Advanced Photon Source for X-ray data collection at Beamline 22ID. The diffraction data were processed using XDS (Vonnrhein et al., 2011). The crystal structure was determined via the method of molecular replacement (McCoy et al., 2007) using coordinates from a previously determined crystal structure (PDB: 4JYT) (Adams et al., 2002, 2010; Goswami et al., 2013). Coot (Emsley and Cowtan, 2004) was used for model building and refinement was done with the PHENIX software package (Adams et al., 2002). A summary of the data reduction and structure refinement statistics are provided in Table S4. Coordinates of the X-ray structure have been deposited in the Protein Data Bank (PDB: 6N4T).

### TMPRSS6 Homology Model Using MOE Modeling

A homology model of TMPRSS6 catalytic domain was built using the structure of matriptase (PDB: 6N4T) with the “Homology Model” module of the Molecular Operating Environment (MOE) from the Chemical Computing Group. Sequence alignment of catalytic domains of matriptase (UniProt: Q9Y5Y6) with TMPRSS6 (UniProt: Q8IU80) using “Align Sequences Protein BLAST” resulted in 45% and 62% sequence identity and similarity, respectively allowing to build a high-quality model. Ten models were created and the final model was selected using the best score obtained by the Generalized-Born Volume Integral/Weighted Surface area (GBVI/WSA) scoring method (Corbeil et al., 2012). The final model was refined and minimized using Amber10: Extended Huckel Theory (EHT) force field.

### Hemojuvelin Cleavage Assay

HepG2 cells were co-transfected in 6-well plates with pcDNA6/V5 or pcDNA6/TMPRSS6-WT-V5 isoform 2/V5 (UniProt Q8IU80-1) and pCMV6-Entry/HJV variant a (UniProt Q6ZVN8-1) using Lipofectamine 3000. 24h after transfection, cell media were replaced with HCell-100 media for another 24h. Cell media was collected, and cells lysed. Cell media was concentrated using centrifugal filters (10,000 NMWL, 21,100 g, 15 min, 4°C). Concentrated samples were loaded on 12% SDS-polyacrylamide gels under denaturing conditions. Migrated proteins were electro-transferred onto nitrocellulose membranes. Nonspecific protein binding was blocked using a solution of 5% bovine serum albumin (BSA) in TBS 0.1% Tween-20. Anti-hemojuvelin antibodies were diluted in a solution of 2.5% BSA in TBS 0.1% Tween-20 and incubated overnight at 4°C. After three sequential washing steps (5 min each) with TBS

0.1% Tween-20, membranes were incubated with horseradish peroxidase-conjugated secondary antibodies (Rabbit anti-Goat) for 1h at RT and washed three times (5 min) in TBS 0.1% Tween-20. Clarity Western ECL substrate was put on membranes and blot images were acquired using a Fusion Pulse system. HJV cleavage fragments intensities were quantified by densitometry analysis using Bio-1D software (Vilber Lourmat) and reported on vehicle-treated cells (0.1% DMSO). Results are expressed as HJV cleavage (%). IC<sub>50</sub> values were derived by a sigmoidal dose-response (variable slope) curve using GraphPad Prism software from a log([Compound]) versus HJV cleavage plot.

### **TMPRSS6 Western Blot**

HepG2 cells were plated on a 96-well plate at a density of 10,000 cells/well in BME media containing serum and supplements. The cells were incubated overnight to allow for cell attachment. Next day, complete media was changed to serum-free media. Depending on the conditions, the cells were then treated with the wild-type or the S762A-mutated TMPRSS6 BacMam or no Bacmam. The cells were incubated overnight. The media was removed from the cells and the cells were washed with PBS twice. The cells were then treated with RIPA lysis buffer with proteinase inhibitor cocktail and incubated for 20 mins on ice with intermittent vortexing. The lysate was collected in tubes and was further sonicated to ensure effective lysis. The lysate was then spun at 1200rpm for 10 mins at 4 degrees. The supernatant was transferred to a separate tube and BCA assay was performed to determine protein quantities. 40ug of protein was loaded onto the gel for each of the conditions. The gel was run and the proteins were transferred on the nitrocellulose membrane. The membrane was incubated overnight with anti-TMPRSS6 antibody to detect TMPRSS6 protein while anti-GAPDH was used as an endogenous control. The blot was washed thrice with TBS-T buffer and then incubated in Licor secondary antibodies for 2 hours and washed with TBS-T buffer. The blot was then scanned with Licor Odyssey scanner.

### **HAMP RT-qPCR**

HepG2 cells were plated on 96-well plate at a density of 10,000 cells/well in BME media containing serum and supplements. The cells were incubated overnight to allow for cell attachment. Next day, complete media was changed to serum-free media. Depending on the conditions, the cells were then treated with wild-type or S762A-mutated TMPRSS6 BacMam. The cells were treated with either DMSO (0.1%) or TMPRSS6 inhibitor compounds (Cpd-8, Cpd-A and Cpd-B) for 6hr, following which the cells were stimulated hBMP6 (3 ng/mL) for 24 hrs. The cell media was collected for Heparin-25 ELISA. Human primary hepatocytes, freshly thawed cells from donors 1797, 1836, 8148 and 8279 were plated on a 96-well plate (15,000 cells/well) in Plating media containing FBS. After 24h, Plating media were replaced by serum free Maintenance media. Cells were treated with either DMSO or 0.1, 1, 5 and 10 μM of Cpd-8, Cpd-A and Cpd-B inhibitor for 6h. Cells were stimulated using hBMP6 (30 ng/mL) for 24 h. The cells (HepG2 or Hepatocytes) were lysed using the lysis buffer from the Cells-to-CT kit for 7 min and the reaction was terminated by adding Stop Solution from the kit. RT-qPCR was performed using the 1-Step TaqMan reagent provided in the kit using the human TaqMan assays for HAMP, B2M and PPIA on the QuantStudio 6flex. The raw data obtained was analyzed using Array Studio software with 2 housekeeper normalization.

### **Heparin Quantification by ELISA**

HepG2 cells were plated on 96-well plate at a density of 10,000 cells/well in BME media containing serum and supplements. The cells were incubated overnight to allow for cell attachment. Next day, complete media was changed to serum-free media with or without TMPRSS6 BacMam. The cells were treated with either DMSO (0.1%) or TMPRSS6 inhibitor compounds (Cpd-8, Cpd-A and Cpd-B) for 6hr, following which the cells were stimulated hBMP6 (3 ng/mL) for 24 hrs. The cell media was collected for Heparin-25 ELISA. Human primary hepatocytes, freshly thawed cells from donor 8279, were plated on a 96-well plate (85,000 cells/well) in Plating media containing FBS. After 24h, Plating media were replaced by serum free Maintenance media. Cells were treated with either DMSO or 0.1, 1, 5 and 10 μM of Cpd-8, Cpd-A and Cpd-B inhibitor for 6h. Cells were stimulated using hBMP6 (5 ng/mL) for 24 hr. Cell media were collected for Heparin-25 quantification and number of viable cells was determined using CellTiter-Glo Cell Viability Assay (CTG) (Promega) on wells attached cells according to the manufacturer protocol. Resulting luminescence was measured using a TriStar<sup>2</sup> LB 942 (Berthold Technologies) microplate reader.

Heparin-25 was assessed in cell media by a competitive ELISA method using the human heparin-25 enzyme immunoassay kit from Peninsula Laboratories following manufacturer protocol (protocol II, for increased sensitivity and signal). After the termination of reactions, absorbance at 450 nm was read with a Tecan Infinite M200 microplate reader. Absorbance of known heparin concentrations (log[Heparin]) was plotted and a standard curve was determined with a sigmoidal dose-response (variable slope) curve using GraphPad Prism software. Samples heparin concentrations was determined using the standard curve. Obtained concentrations were corrected for cell quantity in well according to the number of viable cells determined previously by CTG assay.

### **ID1, SMAD7 and TMPRSS6 RT-qPCR**

Total RNA extractions of human primary hepatocytes (Hu8279) total RNA extractions were performed from plated cells (24-well plate) using TRIzol (Invitrogen) with chloroform as recommended by the manufacturer's protocol. The aqueous layer was recovered, mixed with 1 volume of 70% ethanol, and applied directly to a RNeasy Mini kit column (Qiagen). DNase treatment on the column and total RNA recovery were performed according to the manufacturer's protocol. RNA quality and the presence of contaminating genomic DNA were verified as described previously (Brousseau et al., 2010). RNA integrity was assessed with an Agilent 2100 Bioanalyzer (Agilent Technologies). Reverse transcription was performed on 1.1 μg of total RNA with Transcriptor reverse transcriptase, random hexamers, dNTPs (Roche Diagnostics), and 10 units of RNaseOUT (Invitrogen) following the manufacturer's protocol in a total volume of

10  $\mu$ L. All forward and reverse primers were individually resuspended to 20–100  $\mu$ M stock solutions in Tris-EDTA buffer and diluted as a primer pair to 1  $\mu$ M in RNase DNase-free water. Real-time qPCRs were performed in 10  $\mu$ L in 96-well plates on a CFX-96 thermocycler (Bio-Rad) with 5  $\mu$ L of 2  $\times$  iTaq Universal SYBR Green Supermix (BioRad), 10 ng (3  $\mu$ L) of cDNA, and 200 nM (final concentration; 2  $\mu$ L) primer pair solutions. The following cycling conditions were used: 3 min at 95°C and 50 cycles of 15 s at 95°C, 30 s at 60°C, and 30 s at 72°C. Relative expression levels were calculated using the qBASE framework (Hellemans et al., 2007) and the housekeeping genes YWHAZ, PUM1, and MRPL19 for human cDNA. Primer design and validation were evaluated as described elsewhere (Brosseau et al., 2010). In every qPCR run, a no-template control was performed for each primer pair, and these were consistently negative.

### Statistical Analysis

Statistical values including the number of times the data was replicated (“n”) and statistical significance are reported in the Figure Legends. Statistical analyses were conducted using GraphPad Prism version 7.0c or 8.0.2 (GraphPad Software, La Jolla, CA). Outliers were removed using the ROUT method (Q = 1%). For activity, IC<sub>50</sub> and hemojuvelin cleavage assays, data are represented as the mean  $\pm$  SD and significant differences between groups were determined using non-parametric Kruskal-Wallis test. For RT-qPCR and ELISA results, data are represented as the mean  $\pm$  SEM and significant differences between groups were determined by one-way ANOVA test. For cell surface localization of TMPRSS6 and HJV in HepG2 treated cells, densitometry results are represented as the mean  $\pm$  SEM and significant differences between groups were determined using the one sample t test using 1 (vehicle treated cells value) as hypothetical mean.

### DATA AND CODE AVAILABILITY

The accession number for the matriptase/Cpd-8 structure reported in this paper is PDB: 6N4T.